SMALL SCALE MIXING IN THE INITIAL REGION OF A JET

Final Research Report - 1986

Ephraim Gutmark and I. Wygnanski

Department of Mechanical Engineering

Tel-Aviv University

Tel-Aviv, (Israel)

1. Introduction

Efficient mixing is crucial for the operation of many devices where reaction is taking place, like: chemical reactors, combustors, lasers, etc. The mixing process should not be considered only globally, i.e., in terms of integrated amounts of the mixed components, but rather in terms of the local scales especially the small scales, in order that the molecular mixing between the reactants will increase.

The dominant role of coherent structures in the evolution of free mixing layers has been recognized in many investigations, both at low and at high Reynolds-numbers[1-2]. Much effort was also spent to develop means by which to control these structures actively or passively, in order to augment the mixing process[3]. In hot-flows existing inside combustors, for example, it is preferable to use passive means. The idea of using a non-circular, low aspect ratio nozzle (elliptical or similar shapes) was investigated thoroughly before[3-4]. Such nozzles were tested both in cold flows and while combustion was taking place and proved to be beneficial[3].

SECURITY CLASSIFICATION OF THIS PAGE

REPORT DOCUMENTATION PAGE

1a. REPORT SECURITY CLASSIFICATION UNCLASSIFIED	1b. RESTRICTIVE MARKINGS
2a. SECURITY CLASSIFICATION AUTHORITY	3. DISTRIBUTION/AVAILABILITY OF REPORT APPROVED FOR PUBLIC RELEASE DISTRIBUTION IS UNLIMITED
2b. DECLASSIFICATION/DOWNGRADING SCHEDULE	
4. PERFORMING ORGANIZATION REPORT NUMBER(S)	5. MONITORING ORGANIZATION REPORT NUMBER(S)
6a. NAME OF PERFORMING ORGANIZATION Tel-Aviv University 6b. OFFICE SYMBOL (If applicable)	7a. NAME OF MONITORING ORGANIZATION European Office of Aerospace Research and Developmnet
6c. ADDRESS (City, State and ZIP Code) Ramat Aviv 69978 ISRAEL	7b. ADDRESS (City, State and ZIP Code) Box 14 FPO New York 09510
8a. NAME OF FUNDING/SPONSORING ORGANIZATION EOARD 8b. OFFICE SYMBOL (If applicable) LDV	9. PROCUREMENT INSTRUMENT IDENTIFICATION NUMBER 85-0278
8c. ADDRESS (City, State and ZIP Code) Box 14 FPO New York 09510	10. SOURCE OF FUNDING NOS PROGRAM ELEMENT NO: 61102F PROJECT NO.: 2307 TASK NO.: A2 WORK UNIT NO.:
11. TITLE (Include Security Classification) (U) Small Scale Mixing in Jet	
12. PERSONAL AUTHOR(S) E. Gutmark and I. Wygnanski	
13a. TYPE OF REPORT Final 13b. TIME COVERED FROM 1985 TO 1986	14. DATE OF REPORT (Yr., Mo., Day) 15. PAGE COUNT 40
16. SUPPLEMENTARY NOTATION	
17. COSATI CODES FIELD / GROUP / SUB GR	18. SUBJECT TERMS (Continue on reverse if necessary and identify by block number) Turbulence, Jets, Free Shear Layers, Turbulent Mixing

19. ABSTRACT (Continue on reverse if necessary and identify by block number)

The possibility of achieving substantial mixing enhancement, using noncircular nozzles, was demonstrated. It was shown that nozzle geometries containing sharp corners are beneficial for mixing purposes. By breaking the initial symmetry of the flow, one may also reduce the coherence of the large structures, thus eliminating the main causes for the onset of combustion instabilities.

The excitation of azimuthal instabilities increases the mixing at the higher frequency range. The considerable variation of the mean velocity distribution around the jet, especially near the corners, results in a rapid decrease of the azimuthal cross-correlation near these sections. When such cross-correlation is decomposed into aximuthal modes, higher modes are shown to be present. The higher modes are responsible for the increase in the three-dimensionality of the flow, the turbulence level, and the small scale activity.

20. DISTRIBUTION/AVAILABILITY OF ABSTRACT UNCLASSIFIED/UNLIMITED ☒ SAME AS RPT ☐ DTIC USERS ☐	21. ABSTRACT SECURITY CLASSIFICATION UNCLASSIFIED
22a. NAME OF RESPONSIBLE INDIVIDUAL Maj Thomas E. Speer	22b. TELEPHONE NUMBER (Include Area Code) 01-409-4318 22c. OFFICE SYMBOL EOARD/LDV

DD FORM 1473, 83 APR EDITION OF 1 JAN 73 IS OBSOLETE

SECURITY CLASSIFICATION OF THIS PAGE

The introduction of non-circular ducts with non-conventional geometries could complicate and increase the cost of production. It was, therefore, suggested to study the flow emerging from a regular, circular pipe which is connected to an orifice plate having the desired (non-circular) nozzle geometry. For this purpose one had to study the flow characteristics of such jets and compare them to regular jets emerging from well designed nozzles[5].

The present report describes the results of an experimental and theoretical investigation done using five orifice nozzle configurations: a regular elongated slot with a 3:1 aspect-ratio (Slot Jet), a similar slot having a conical contraction (Tapered Slot Jet), a square nozzle, an equilateral triangular nozzle, and a circular jet.

2. Experimental Set Up

The experimental set-up consist of a free jet with interchangeable orifice nozzles. Five different shapes of nozzles are studied: circular, triangular, square, an elongated slot, and a tapered slot jet.

The circular jet had an exit diameter of 5 cm. The equilaterial triangular orifice and the square orifice had the same exit area. The elongated slot consisted of a rectangle with two half circles at its small sides. The slot width was 2 cm and length 6 cm, yielding an aspect ratio of 3:1. The tapered slot-jet had the same outlet shape, with a conical area contraction of 9:1.

The circular, triangular, and square nozzles have a small circular bell mouth of 10 mm radius on the inner surface of the orifice plate to prevent the

separation of the flow at the inlet. The slot nozzle does not have any bell mouth at all. The tapered slot nozzle had a conical contraction with an inlet diameter equal to major axis of the slot while the outlet diameter is equal to the minor axis of the slot.

The air is supplied by a radial blower, which is attached to a diffuser by a flexible hose. The air then passes through a cubic chamber, which also houses a loudspeaker, providing controlled perturbations to the flow. The main settling chamber, further downstream has, however, a circular cross-section. This chamber is 500 mm long and contains a honeycomb and two screens (Figure 1). The jet exit velocity, U_o, can be varied between 2 m/s and 50 m/sec, corresponding to a variation in Reynolds number of $6 \cdot 10^5$ to $1.7 \cdot 10^5$.

Hot-wire anemometers are used for probing the flow field, the measurements included mean velocity profiles, the distribution of turbulent intensities, spectral analysis, cross-correlations, and the determination of eigenfunctions and phase distributions across the jet at various axial positions. A lathe x-y table was used as a traverse-mechanism, controlling the axial and radial positions of the measuring probe.

The hot-wire calibration, the data acquisition, and analysis were done on a PDP 11/60 minicomputer. The flow was visualized using smoke illuminated by a Strobe which was sunchronized with the forcing frequency which was set to match the dominant unstable frequency in the flow. The forcing perturbations are generated by a speaker, activated by a signal coming from a function-generator (Krohn-Hite model 5200) and passing through a power amplifier (Tonar A120X).

3. Results and Discussion

3.1. The Flow Produced by a Triangular Nozzle

The nozzle used had a shape of an equilateral triangle with an equivalent diameter (D_e) of 5 cm.

The mean velocity profiles produced by the triangular jet are shown in Figure 2. The right side of the figure represents the shear layer originating from the flat side of the triangle. The opposite side describes the shear layer at the apex. The different behavior of the mean flow at the opposite sides of the figure results from very different instability characteristics. The initial shear layer is thicker at the apex, but the spreading rate of the jet is higher on the flat side, (i.e., near the center of the nozzle-wall) resulting in an eventual evolution of the triangular jet to a quasi axisymmetric jet at about 5 D_e. The shear layer instability produces a substantial difference in the turbulence activity of the jet on the two sides considered (Figure 3). The initial turbulence level at the apex is about 5 times higher than on the flat side. This turbulence contains a broadband of frequencies (Figure 4) indicating a strong activity in both large and small scales, which is advantageous for enhancing molecular mixing during the combustion process.

The turbulence growth rate is much higher on the flat side than near the apex. In the vicinity of the apex the turbulence level remains almost constant (Figures 3 and 4).

The maximum turbulence intensity at the flat side and near the apex are compared in Figure 5 at numerous downstream distances. Also shown in this figure is the increase in the turbulence activity in the potential core of the jet. At the nozzle exit the level of turbulence is less than one percent of the mean velocity. It attains a maximum at X=5 D_e at a level of 20 percent. The turbulence level at the corner of the square nozzle is included in Figure 5. Its initial level is lower than near the apex of the triangle, indicating that the turbulent intensity increases when the angles of the nozzle walls are smaller. The turbulence level which is similar to the level observed near the triangle apex remains at the same value for different axial positions.

Contrary to the broadband spectral distribution at the apex (Figure 4a), the spectral distribution of the turbulence on the flat side has distinct peaks (Figure 4b), the highest peak occurs at 784 Hz and is about 100 times more energetic than the background turbulence. This peak represents the energy of the coherent structures which dominate the shear layer on this side of the nozzle, as opposed to the broadband turbulence observed near the apex. This difference is also demonstrated in Figure 6, where smoke visualization shows that coherent vortices are shed from the flat side while highly turbulent flow characterizes the shear layer near the apex. These results show that the coherent structures which regularly emerge from a circular nozzle causing, as explained before, the combustion instability, may disintegrate near the apex of a triangular nozzle. This important result is demonstrated by compairing radial and axial cross-correlations measured in circular and in triangular jets (Figure 7, taken from Reference 6). The cross-correlations in the circular jet exhibit sinusoidal behavior, characteristic to a highly coherent-periodic flow.

The cross-correlation between the apex and the flat side of the nozzle versus the irregularity of the flow near the apex is depicted again in Figure 7b.

The difference between the spreading rates on the flat and vertex sides of the triangle are shown in Figure 8. The flow at the flat side spreads out, while at the vertex side the jet contracts at the first two diameters and remains almost constant up to 14 diameters from the nozzle.

As a result of this difference the initial triangular shape of the jet cross-section (Figure 9a and b) evolves into a quasi circular shape at 0.4 diameters (Figure 9c) and into a reversed triangle at 1 D_e (Figure 9d). Even at a distance of $7D_e$ from the nozzle, the jet does not "recover" from the higher spreading rate of the flat side and has a reversed triangular shape.

3.2. Square Jet

Many observations which were made in the trianguler jet are repeated in the square jet, except that in this case, as a result of the larger vertex angle, the differences between the flat and vertex side are less emphasized. The initial shear layer at the vertex side had a higher turbulent intensity than that on the flat side (Figure 10a). The growth rate at the flat side is much higher as a result of the large spreading rate (Figure 10a) so that at $x/D_e > 1$ the intensity at the flat side becomes higher. The jet cross-section shape switching, which was observed in the triangular jet occurs in the square jet too. The initial square shape (Figure 11a) as indicated by the mean velocity contour plot becomes quasi circular very close to the nozzle ($x/D_e = 0.2$, Figure 11b) and then is inverted at $0.7D_e$ (Figure 11c). The large spread of

the flat side continues up to $4D_e$ where it saturates and remains contant (Figure 10b). At this location the vertex side resumes its growth, but at a lower rate and only at $14D_e$ the two sides are equal in diameter (Figure 11d).

The mean velocity profiles and the turbulence fluctuation level measured at different downstream distances at the flat and vertex sides of the square jet are given in Figures 12 and 13.

3.3. Slot Jet

The use of a small-aspect-ratio elliptical nozzle for passive control and enhancement mixing was described previously[3,7]. Similar behavior was found for the more elongated 3:1 aspect ratio slot embedded in an orifice plate, without any added contraction. The mean velocity profile measured along the long and short sides of the slot are plotted in Figures 14a and b. The jet spreads out along the narrow side and contracts along the slot length.

This is shown again in Figure 15, where the location of the half width of the jet in both planes is compared. The width in the plane of the minor axis, which is three times narrower at the exit, increases almost linearly and becomes equal to the jet width in the other plane at $X = 2D_e$. The width of the jet in the plane of the major axis decreases, in the initial region, continuously with X and beyond $X = 2D_e$ the major axis becomes the minor one and vice versa. One more switch of the axes occurred at $10D_e$. Mean velocity contours of the flow at various axial cross-sections are shown in Figure 16. The evolution of the axial component of the turbulent intensity profiles on the two orthogonal planes of the jet are shown in Figures 17a and b.

The maximum intensity at X = 5 mm in the shear layer is slightly higher on the major axis shear layer and its level remains higher further downstream. The specific growth pattern of the jet in the two planes is reflected also in the diffusion of turbulence. As a reference for the data described in the next section, it should be noted that the increase in the level of turbulence in the core of the jet is relatively slow.

The instability characteristics of the jet were both measured and calculated using the two dimensional Rayleigh equation[7]. The mean velocity profiles were fitted with a combination of a tanh profile and its higher derivatives. The resulting spatial growth rate α_i as a function of the Strouhal number, $\omega\theta/U_o$, is shown in Figure 18. The phase velocity of the different frequencies is given in Figure 19 showing the dispersive and non-dispersive regions of the unstable frequencies. The derivative of the eigenfunction which corresponds to the most amplified frequency is shown in Figure 20. The phase variation across the shear layer was calculated too. The measured and calculated results compared well.

3.4. The Tapered Slot Jet

The low level of turbulence in the core of the above described slot jet is considered a drawback when a high mixing rate is required in the entire flow field for the purpose of enhancing mixing in the entire reactor. In order to overcome this problem, a special contraction was added, aimed at distorting the outflowing vortices and adding a new source of axial vorticity generation thus producing an additional instability source and enhanced mixing. The velocity profiles of the tapered slot nozzle are shown in Figures 21a and b. A

drastic change in the flow behavior is obtained. The spreading rate on the side of the minor axis is reduced considerably, while the growth along the major axis is increased substantially (see also Figure 22). Starting from $X = 1.5D_e$ a hump in the velocity profile in the plane of the major axis is generated. The effects ensuing from this type of mean velocity distribution on the generation of turbulence are shown in Figures 23a and b where the radial distributions of the axial component of the turbulence intensity are plotted. The high turbulence activity in the shear layer, i.e., at the jet periphery is maintained, but in addition the turbulence in the core of the jet is augmented considerably. This is a direct result of the generation of axial vorticity component. The variation of turbulence level along the axis of the regular and the tapered slot nozzles is compared in Figure 24. The turbulence level of the tapered nozzle can be five times higher than in the corresponding untapered nozzle. The increase in the level of turbulence along the axis of a circular jet is given, for comparison, in this figure. The introduction of the azimuthal disturbances into the initial shear layer of the jet issued from the tapered slot nozzle results in a very complicated flow field as is demonstrated by the flow visualization results (Figure 25). The flow is unstable to numerous azimuthal modes leading to an eventual breakdown of the flow to small scale turbulence, thus enhancing the mixing at the smaller scales. The complexity of this flow field and its dependence on the azimuthal location is demonstrated by three power spectra of the jet velocity, taken in the shear layer along the major and the minor axes and at an intermediate point between them (Figure 26a, b, and c). The broadest spectrum characterizes the side of the major axis. The minor axis side has a higher rate of roll-off at the high frequencies, without any distinct peaks. The mid point has a high and relatively narrow peak which is about 70 times more energetic than the background.

4. Conclusions

The possibility of achieving substantial mixing enhancement, using noncircular nozzles, was demonstrated. It was shown that nozzle geometries containing sharp corners are beneficial for mixing purposes. The initial turbulence intensity is considerably higher at the small angle section, thus it should be the best location for intense initial mixing. On the other hand, by breaking the initial symmetry of the flow it is possible to reduce the cherence of the large structures thus eliminating the source that causes the onset of combustion instabilities.

An improved slot nozzle with a conical contraction section was proven to be able to enhance the turbulence level in the entire jet. This was achieved by onsetting additional source of axial vorticity instabilities in the initial region of shedding vortices. It was also shown that jets emerging from an orifice plate have similar characteristics to regular jets and can be used (i.e., following a well designed contraction) in order to simplify the application of special nozzle-geometries in real systems.

The excitation of azimuthal instabilities increases the mixing in the higher range of frequencies. The considerable variation of the mean velocity distribution around the jet, especially near the corners, yields a rapid decrease in the azimuthal cross-correlation near these sections. When such cross-correlatio distribution is decomposed into azimuthal modes, high modes are present. The higher modes increase the three dimensionality of the flow and the turbulence small scale activity.

Most previous investigators concentrated on the evolution of temporal and spatial instabilities in two dimensions (i.e., the flow was considered to be plane or axially symmetric). The introduction of noncircular initial conditions results in the generation of azimuthal modes of the instability. These modes presumably interact and produce new waves via subharmonic resonance and other nonlinear interactions. In order to understand the mechanisms governing the evolution of the flow for future optimization of the design of such nozzles, theoretical and experimental investigations are needed on the different geometries of noncircular jets.

The main parameters which were identified as the ones having the strongest effect on the dynamics of the initial mixing region are: the velocity ratio between the jet and the ambient air, the turbulent or laminar initial conditions, the shape of the mean velocity profile and Reynolds number.

The present work was done at low Reynolds numbers (30,000), which simplifies the measurements and the acquisition of data, but for purpose of application it is important to extend the measurements to Reynolds numbers which are one or two orders of magnitude larger. Design considerations of different combustors require a variety of velocity ratios to be considered, thus a jet discharging into a secondary stream has to be investigated too. In actual applications the laminar initial conditions, so typical to laboratory jets, do not exist. It is therefore important to study the effects of turbulent initial conditions on the development of the flow.

The nonregular nozzles used in this research produce mean velocity profiles, which are sometimes very different from the regular jet profiles

encountered in the literature, which can be expressed by a simple function like the tanh profile. Since the jet stability is highly sensitive to the detailed shape of the mean profile, this aspect should be investigated carefully.

Bibliography

1. Brown and Roshko, J.F.M., 64, 775, 1974.

2. K. C. Schadow, K. J. Wilson, J. E. Crump, and E. Gutmark, AIAA paper No. 84-0530, 1984.

3. K. C. Schadow, K. J. Wilson, M. J. Lee, and E. Gutmark, AIAA paper No. 84-1260, 1984.

4. E. Gutmark, K. C. Schadow, and K. J. Wilson, AIAA paper No. 85-0543, 1985.

5. Michalke, Progress in Aerospace Sciences, 12, Pergamon-Press, 1972.

6. K. C. Schadow, K. J. Wilson, D. M. Parr, C. J. Bicker, and E. Gutmark, AIAA paper No. 85-1109, 1985.

7. C. M. Ho and E. Gutmark, J.F.M., 1986.

Figure 1. Experimental Set-Up.

Figure 2. Mean Velocity Profiles Across the Triangular Jet.

Figure 3. Axial Turbulence Intensity Across the Triangular Jet.

Figure 4. Spectral Distribution of the Turbulent Fluctuations.

Figure 5. Turbulence Intensity Variation Along the Axis of the Triangular and Square Jets.

Figure 6. Smoke Visualization of the Triangular Jet.

Figure 7a. Radial Cross-Correlations in the Circular and Triangular Jets.

Figure 7b. Longitudinal Cross-Correlations in the Circular and Triangular Jets.

Figure 8. Spreading Rate at the Flat and Vertex Sides of the Triangular Jet.

Figure 9. Mean Velocity Controus of the Triangular Jet at Different Axial Locations.

Figure 10. Comparison of Square Jet Spreading Rate and Maximal Turbulence Intensity at the Flat and Corner Sides.

Figure 11. Mean Velocity Contours of the Square Jet at Different Axial Locations.

Figure 12. Mean Velocity Profiles at the Flat and Vertex Sides of the Square Jet at Different Axial Locations.

Figure 13. Turbulence Intensity Profiles at the Flat and Vertex Sides of the Square Jet at Different Axial Locations.

Figure 14a. Mean Velocity Profiles of the Slot-Jet, Minor Axis Plane.

Figure 14b. Mean Velocity Profiles of the Slot-Jet, Major Axis Plane.

Figure 15. Half Width Variation With Downstream Distance in Slot-Jet.

Figure 16. Mean Velocity Contours of the Slot Jet at Different Axial Cross Sections.

Figure 17a. Turbulence Intensity Profiles in the Slot-Jet, Minor Axis Plane.

Figure 17b. Turbulence Intensity Profiles in the Slot-Jet, Major Axis Plane.

Figure 18. Amplification Curve: Spatial Growth Rate ($-d_1$) dependence on the Strouhal Number $W\theta/U_o$.

Figure 19. Phase Velocity Variation with Strouhal Number - $W\theta/U_o$.

Figure 20. ϕ' Distribution Across the Shear Layer at the Minor Axis Plane.

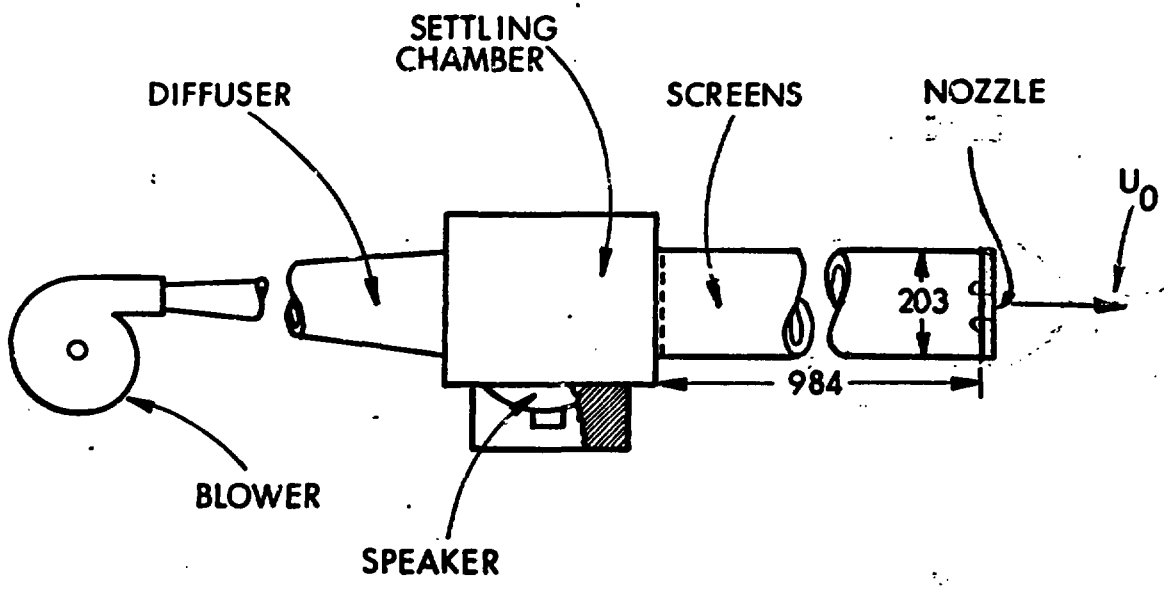
SETTLING
CHAMBER
DIFFUSER
SCREENS
NOZZLE
U_0
203
984
BLOWER
SPEAKER

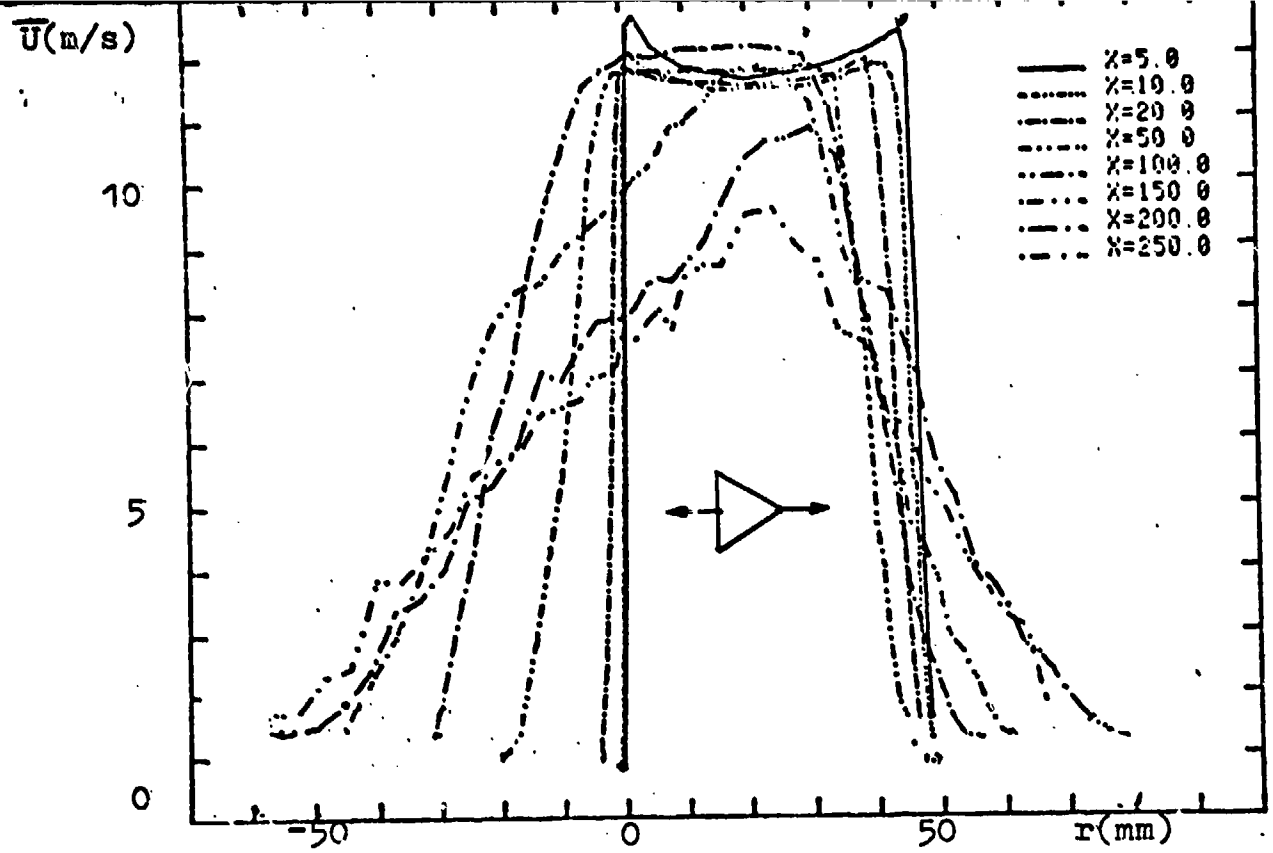

Figure 2: Mean velocity profiles across the triangular jet.

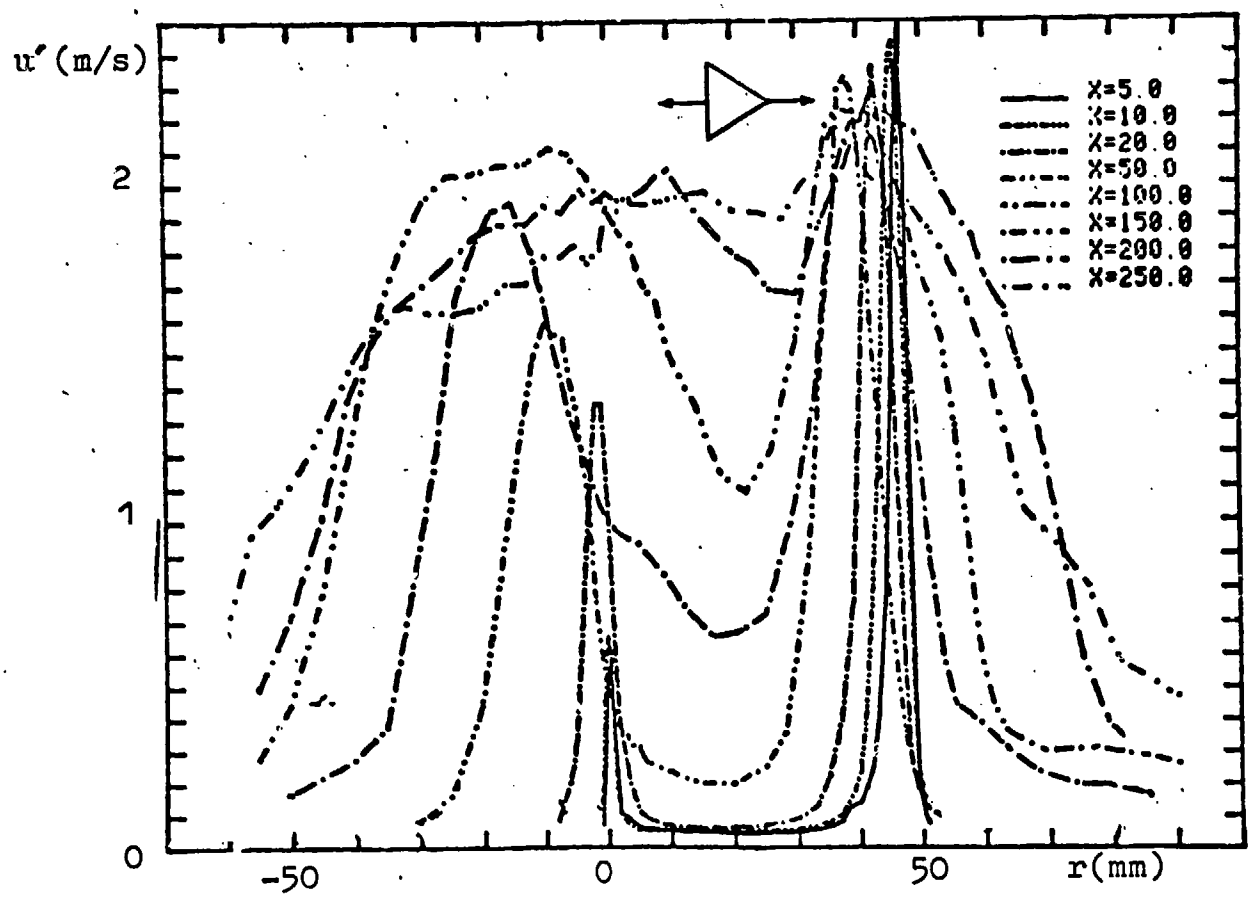

Figure 3: Axial turbulence intensity across the triangular jet.

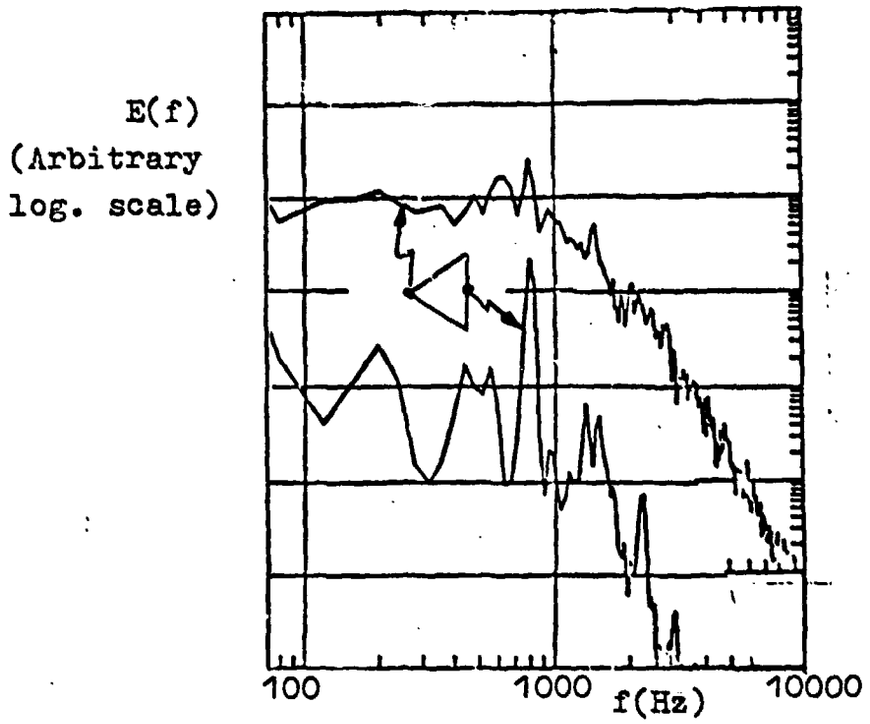

Figure 4: Spectral distribution of the turbulent fluctuations.

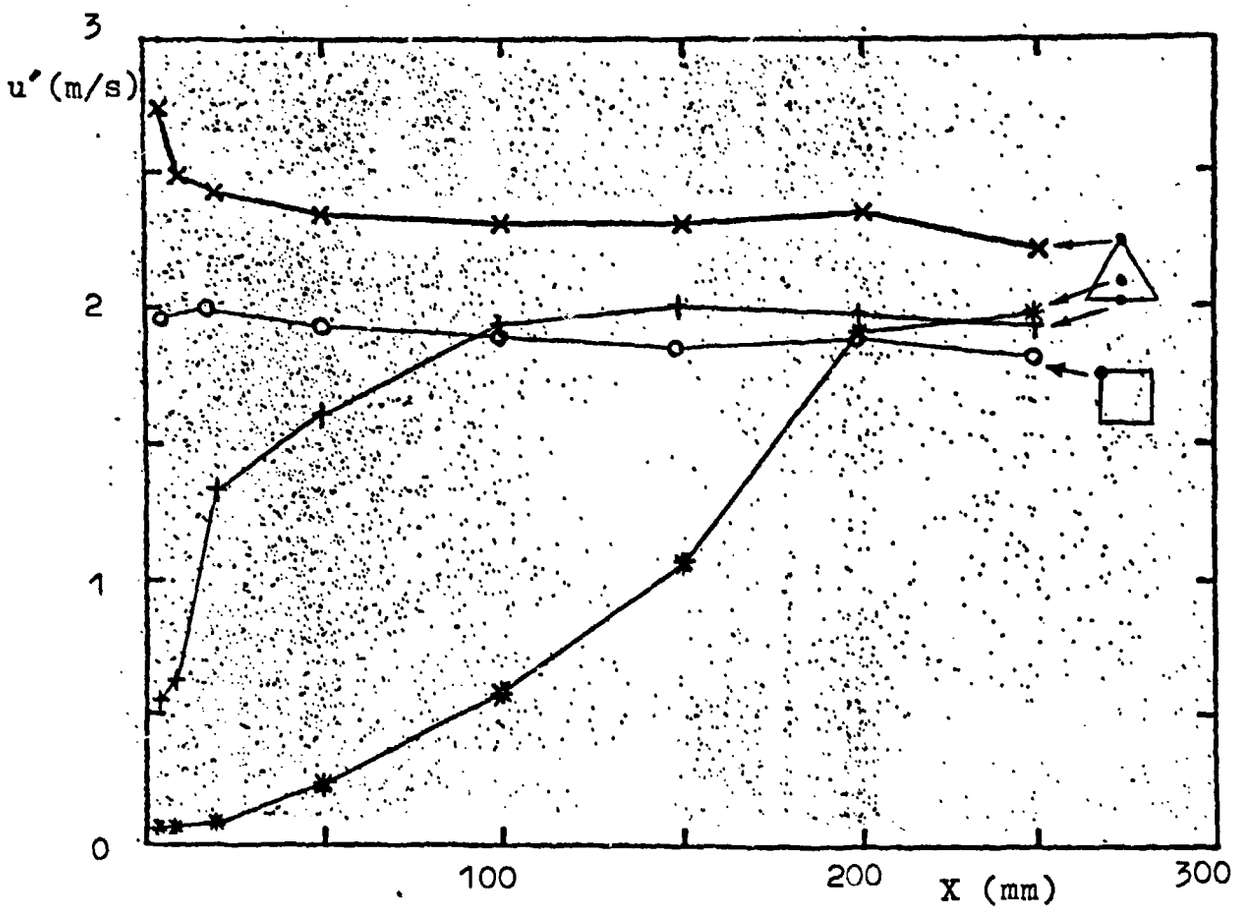

Figure 5: Turbulence intensity variation along the axis of the triangular & square jets.

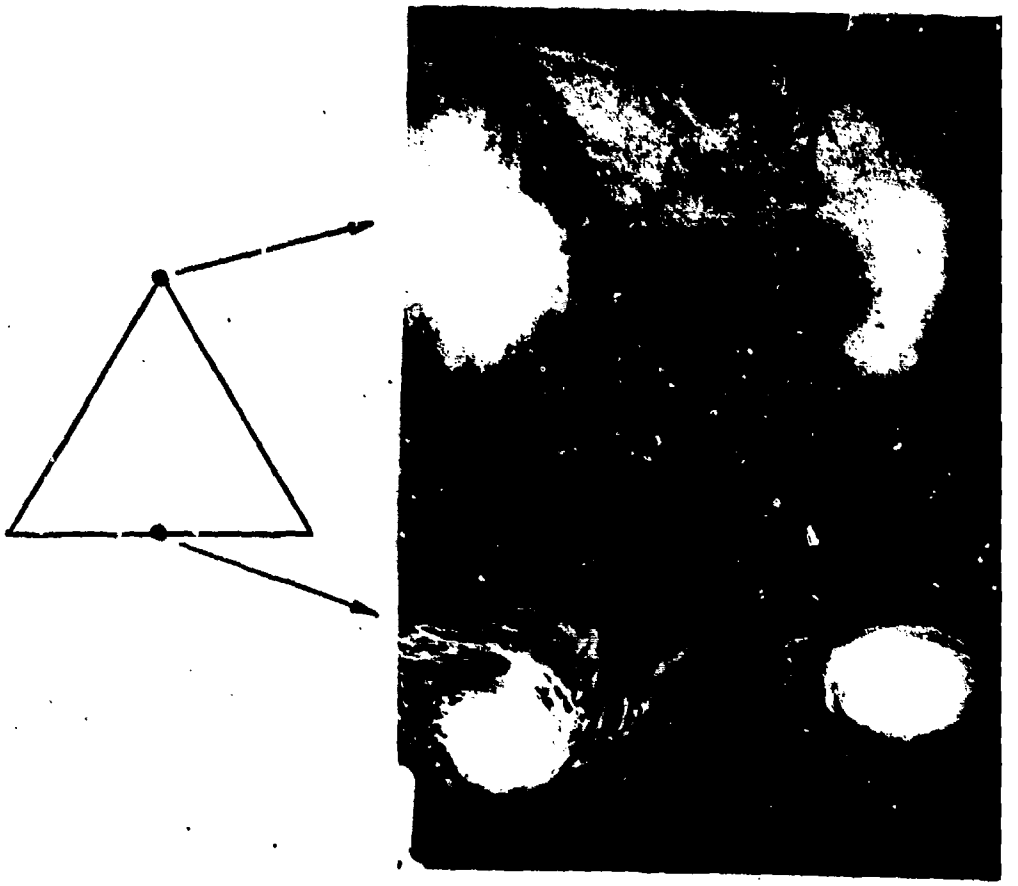

Figure 6: Smoke visualization of the triangular

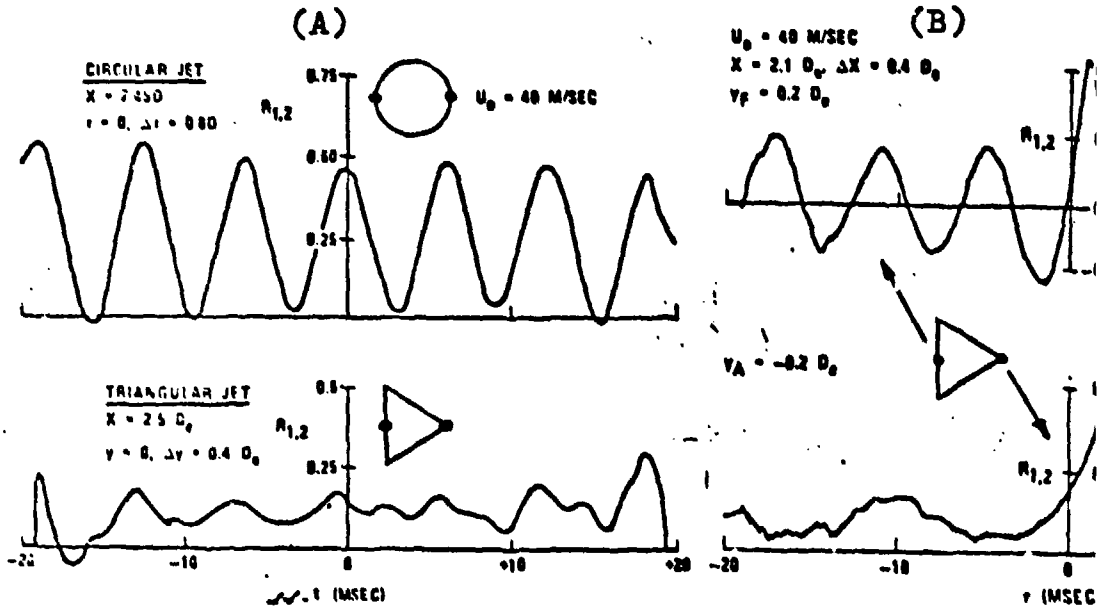

Figure 7: Radial (A) and longitudinal (B) cross
in the circular and triangular jets.

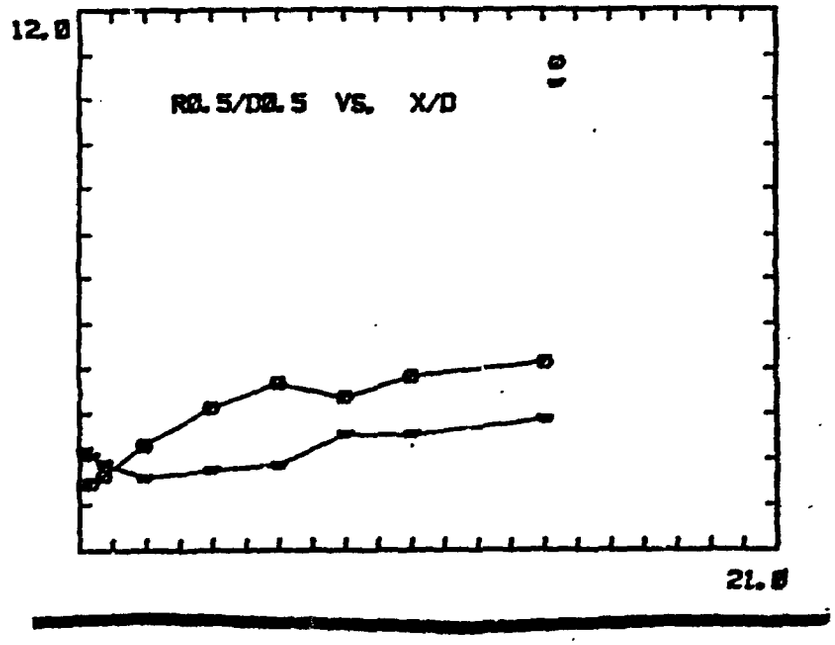
12.0
RØ.5/DØ.5 VS. X/D
21.0

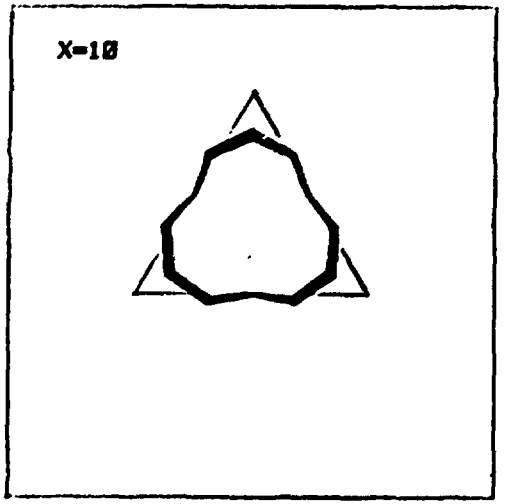
X=10

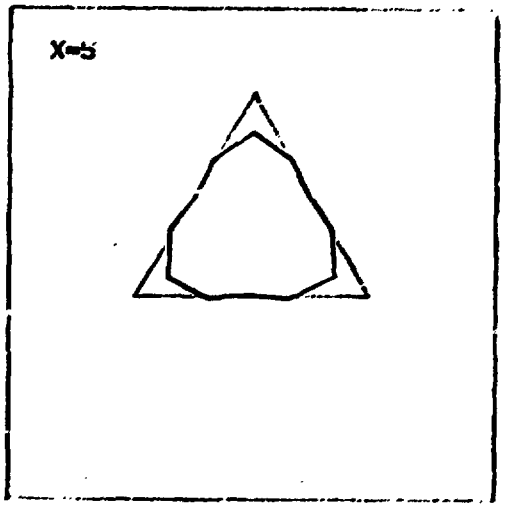
X=5

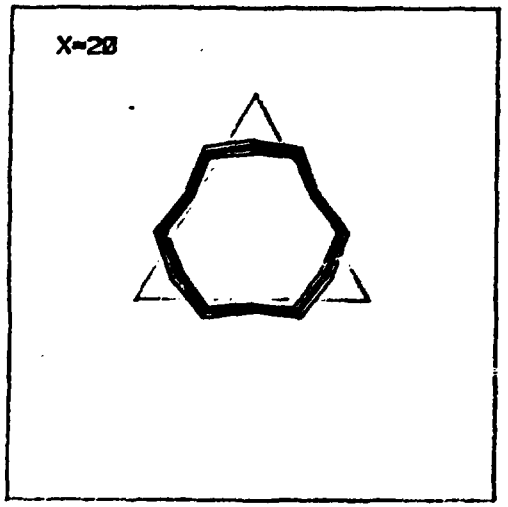
X=20

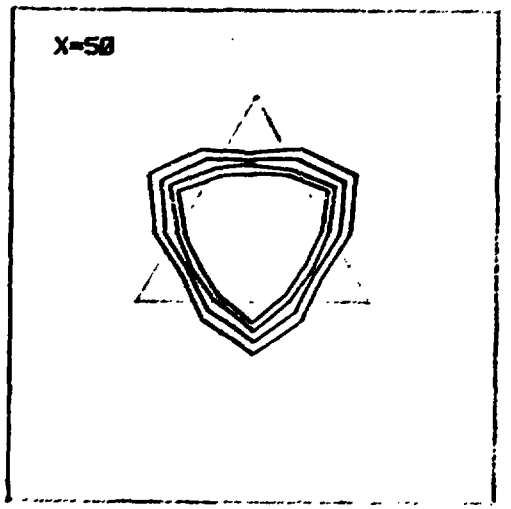
X=50

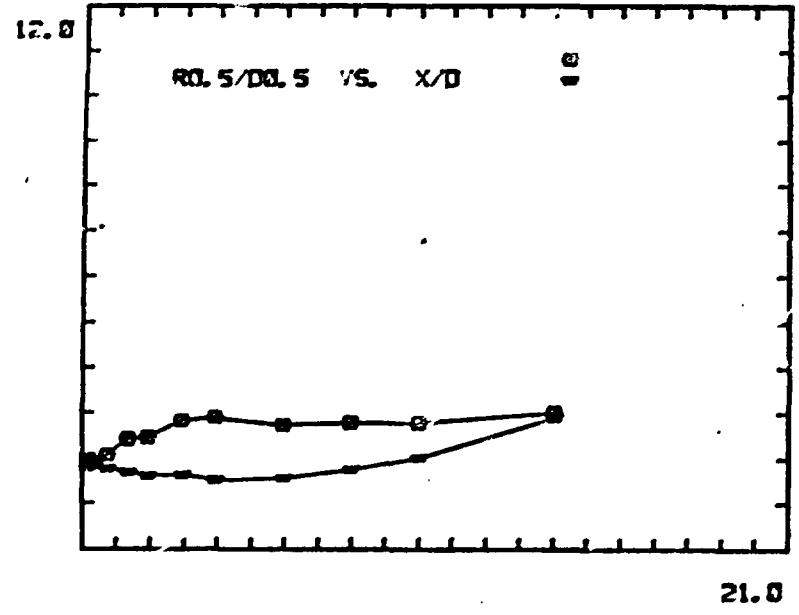
12.0
RO.5/DO.5 VS. X/D
21.0

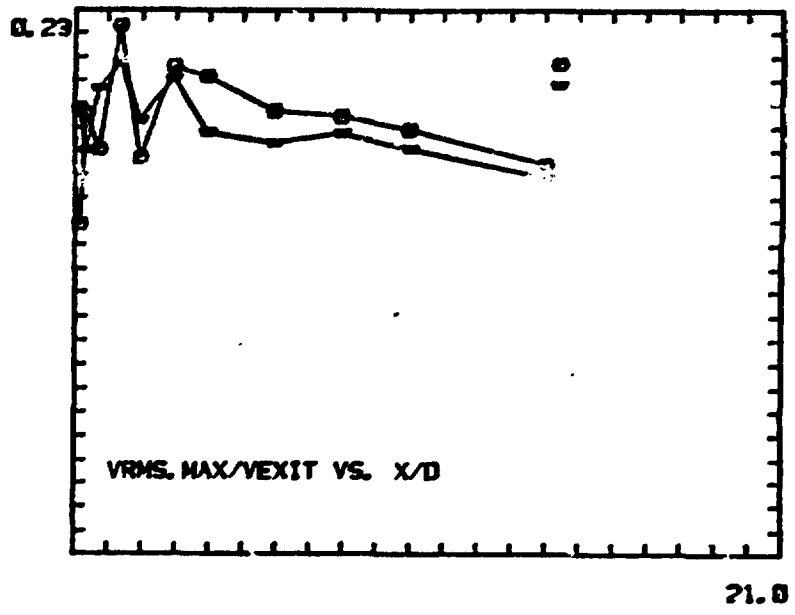
0.23
VRMS.MAX/VEXIT VS. X/D
21.0

b

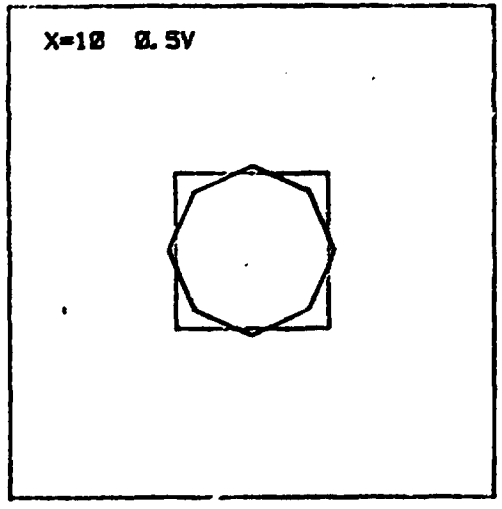

a

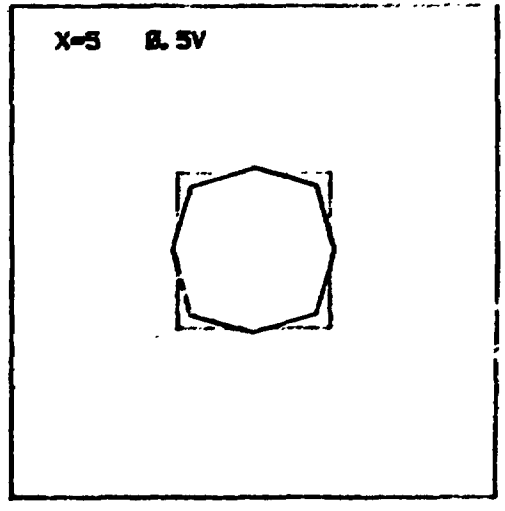

d

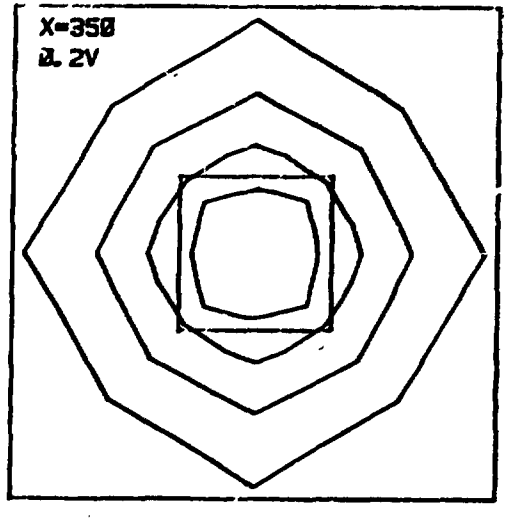

c

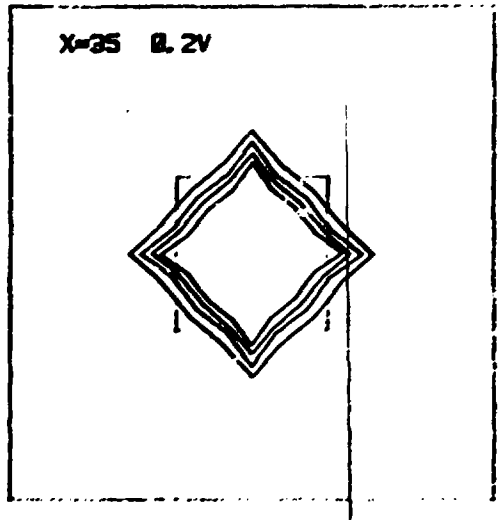

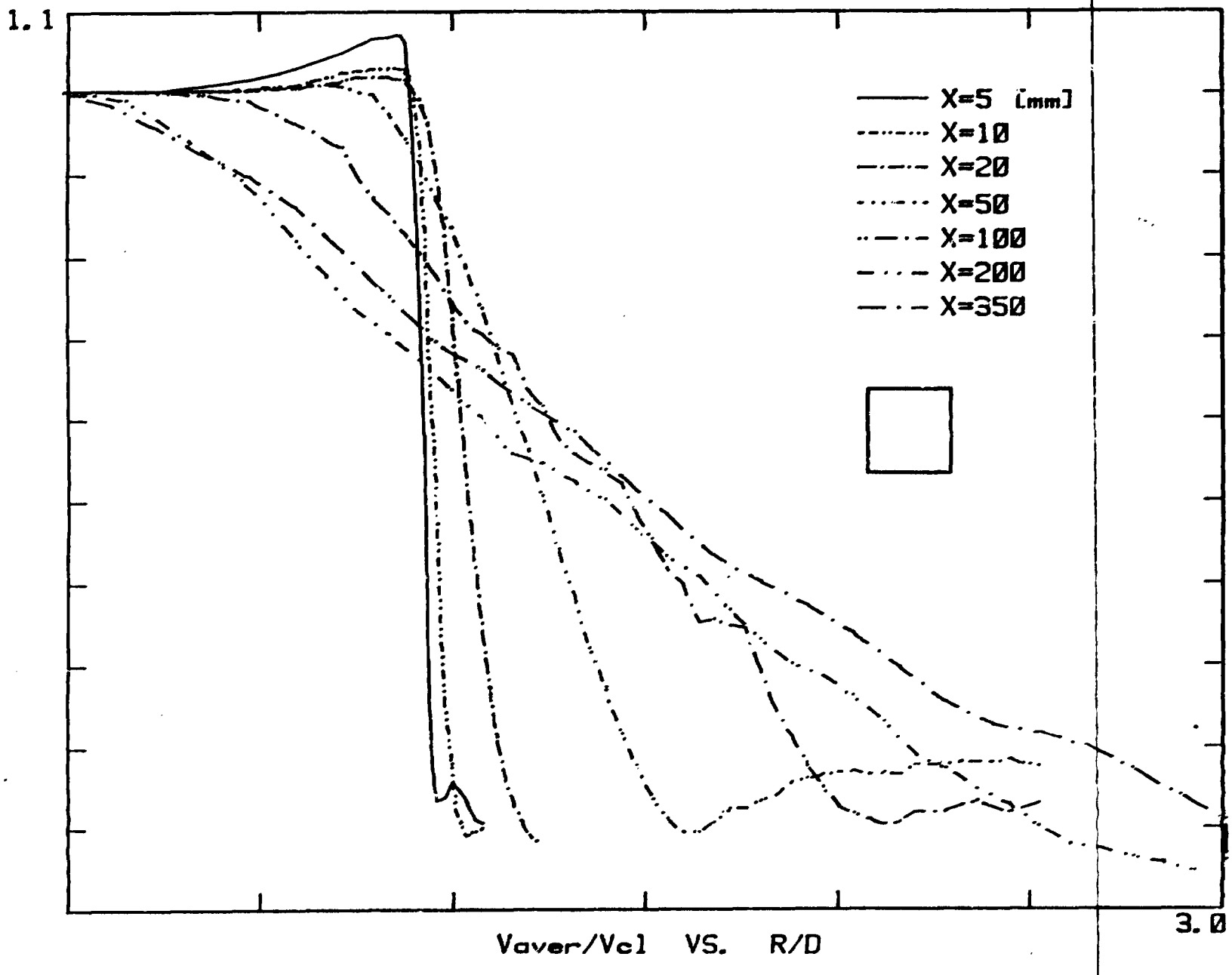
1.1
X=5 [mm]
X=10
X=20
X=50
X=100
X=200
X=350
3.0
Vaver/Vc1 VS. R/D

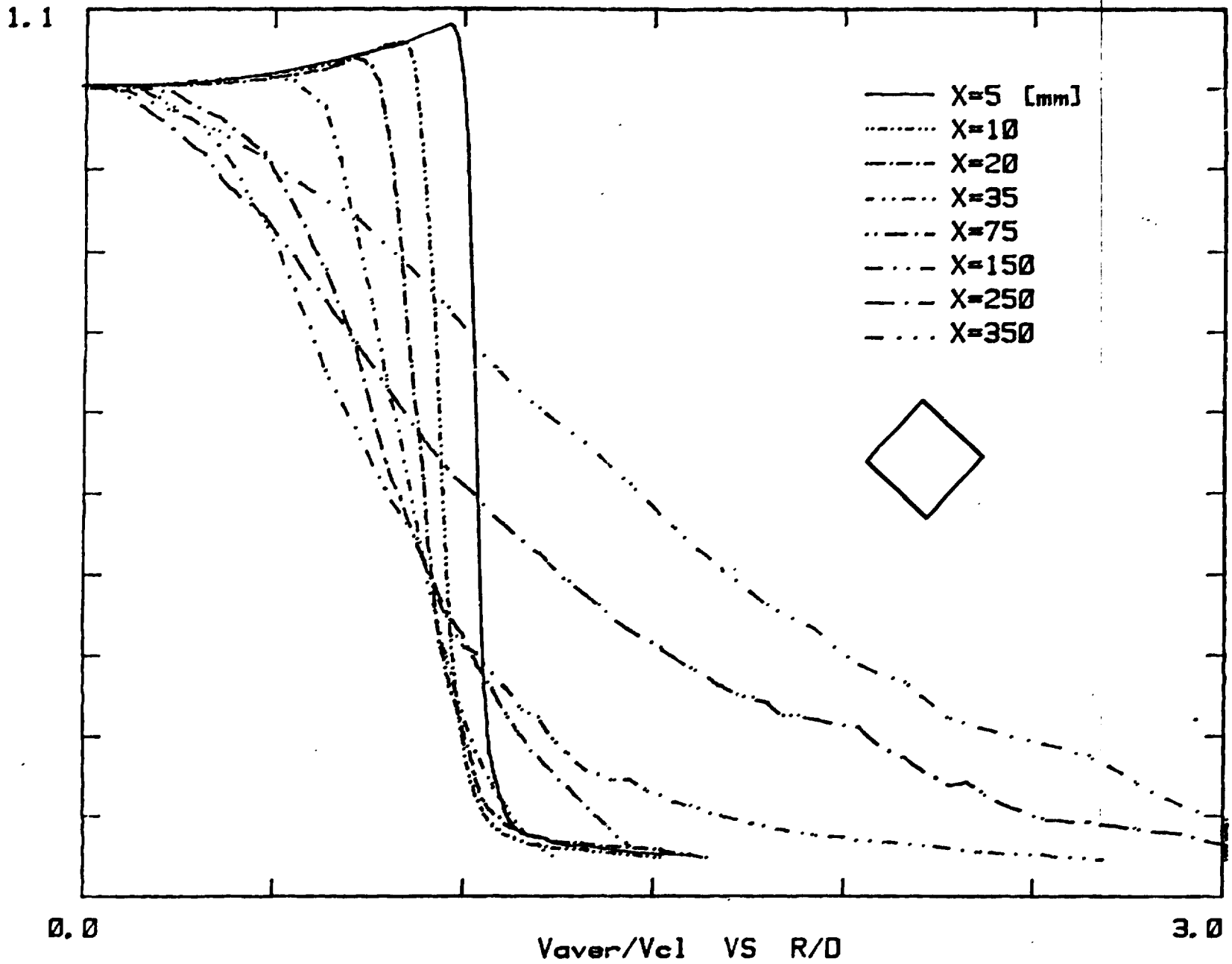
1.1
X=5 [mm]
X=10
X=20
X=35
X=75
X=150
X=250
X=350
0.0
3.0
Vaver/Vcl VS R/D

3a

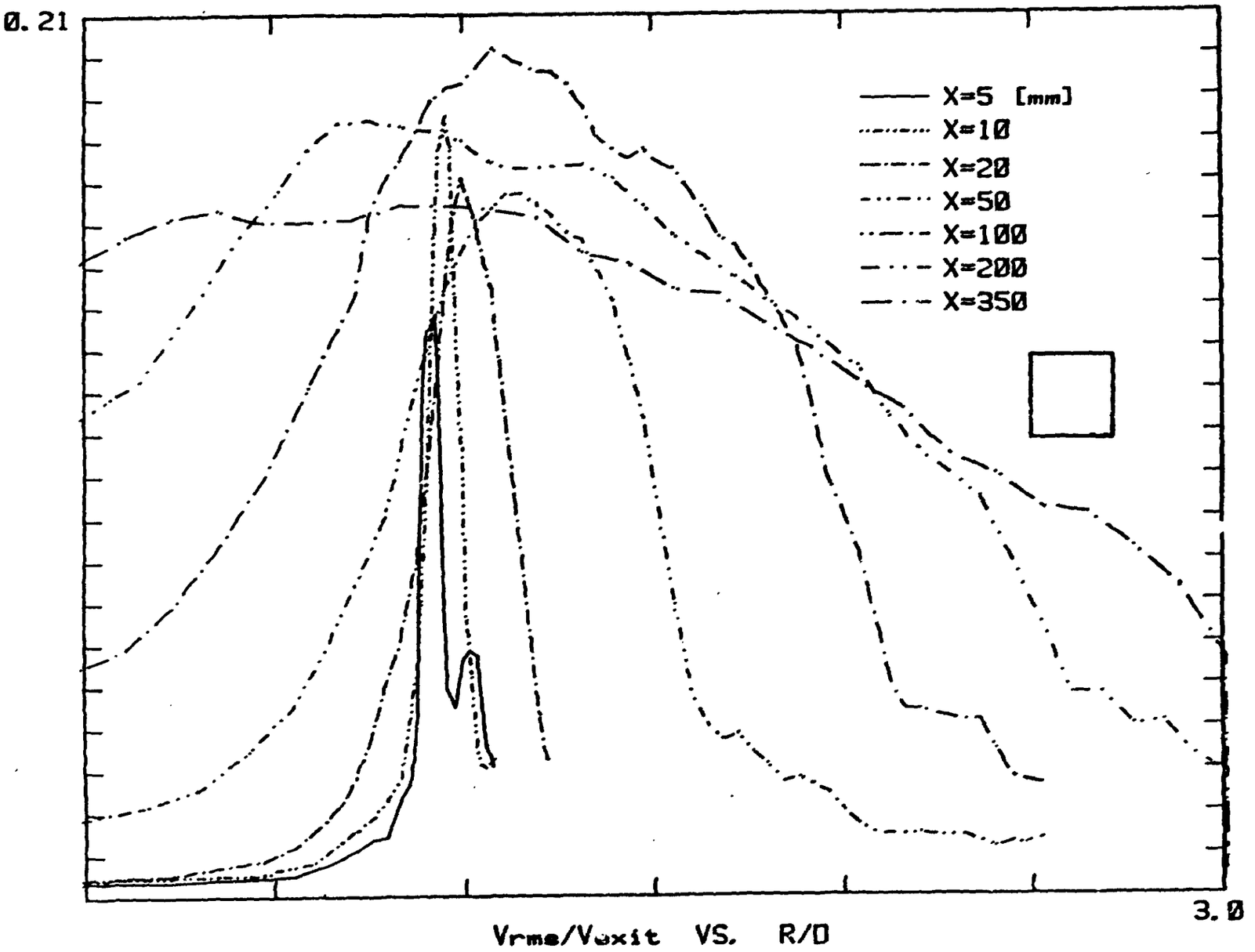

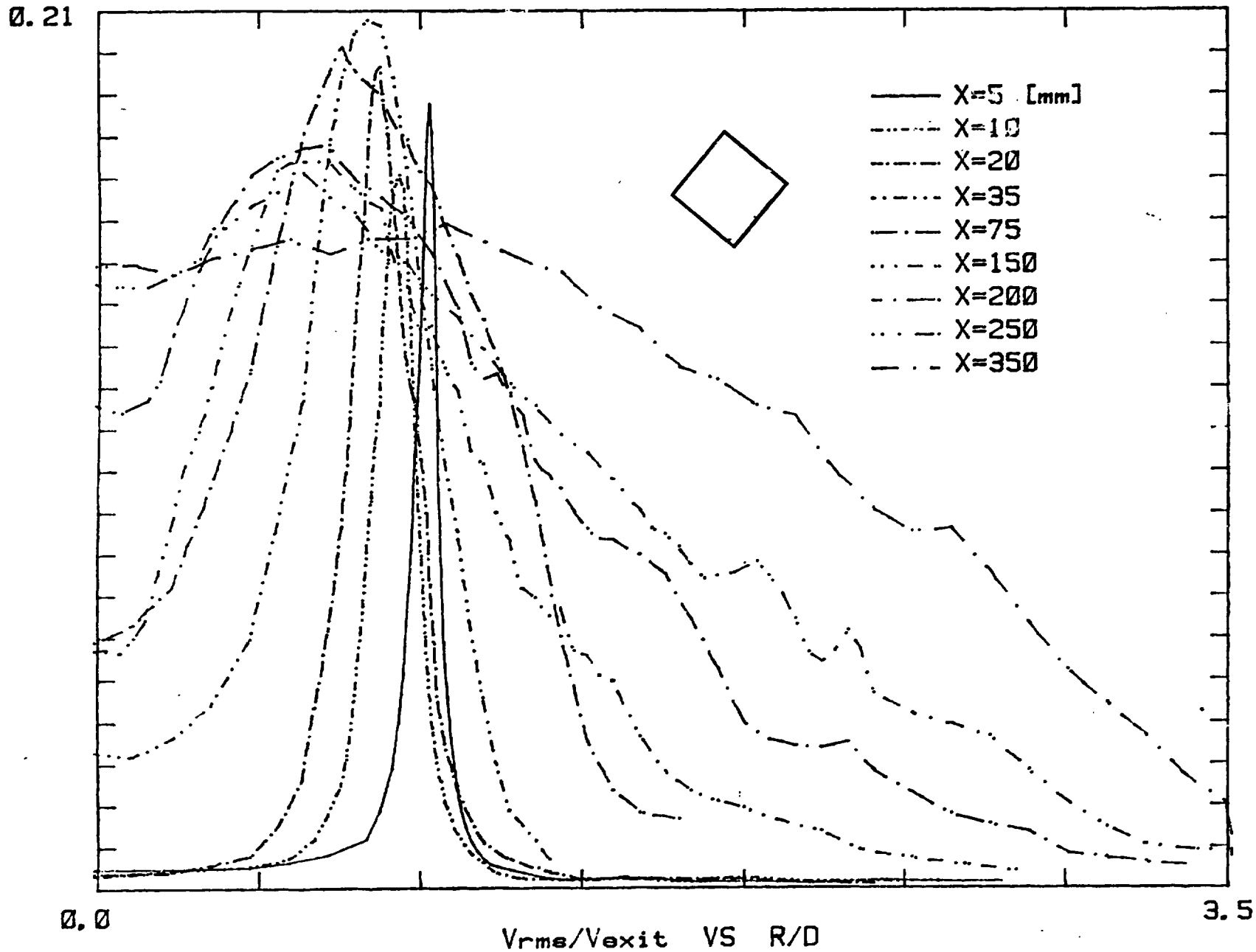
0.21
0.0
3.5
X=5 [mm]
X=10
X=20
X=35
X=75
X=150
X=200
X=250
X=350
Vrms/Vexit VS R/D

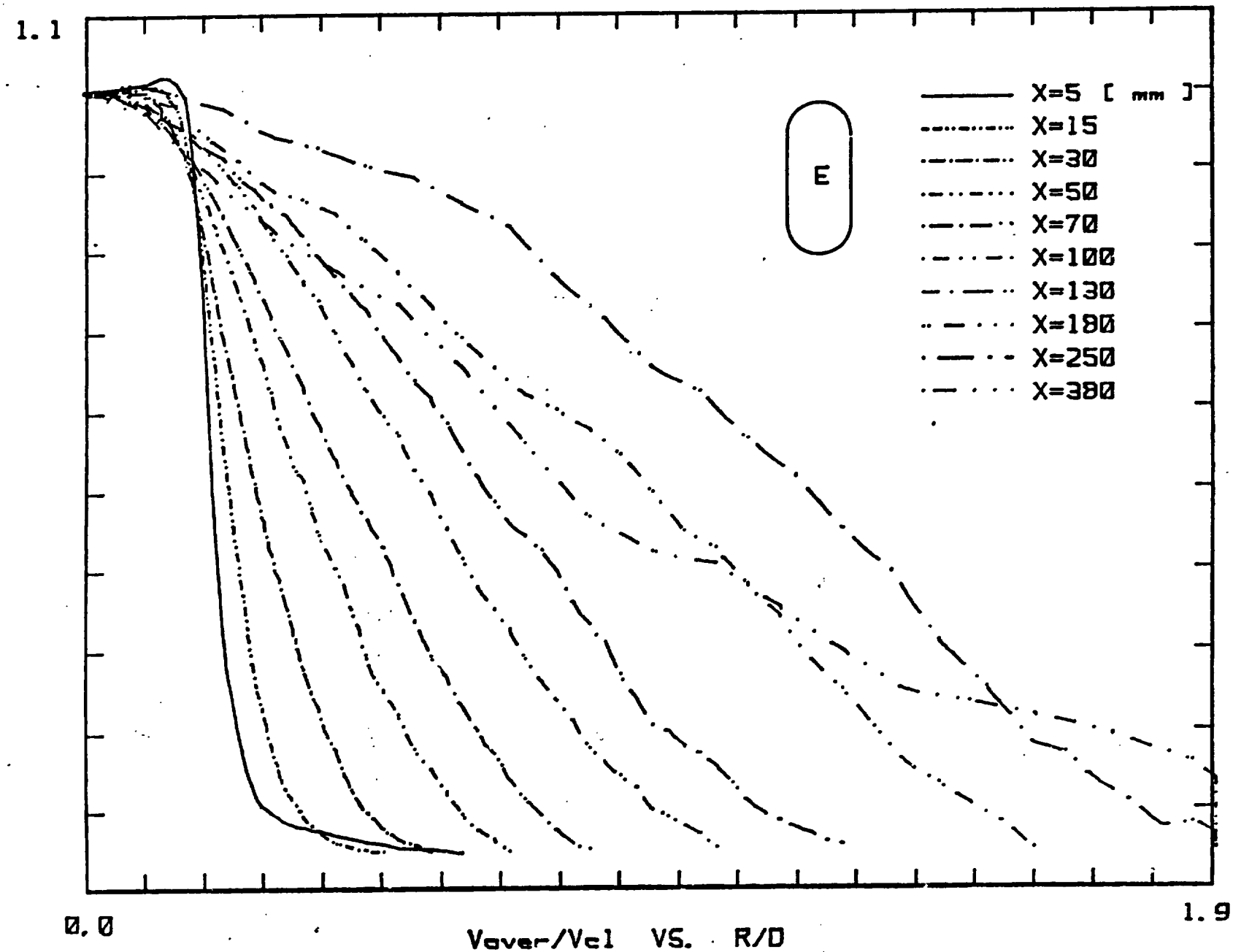

Figure 14a. Mean Velocity Profiles of the Slot-Jet, Minor Axis Plane.

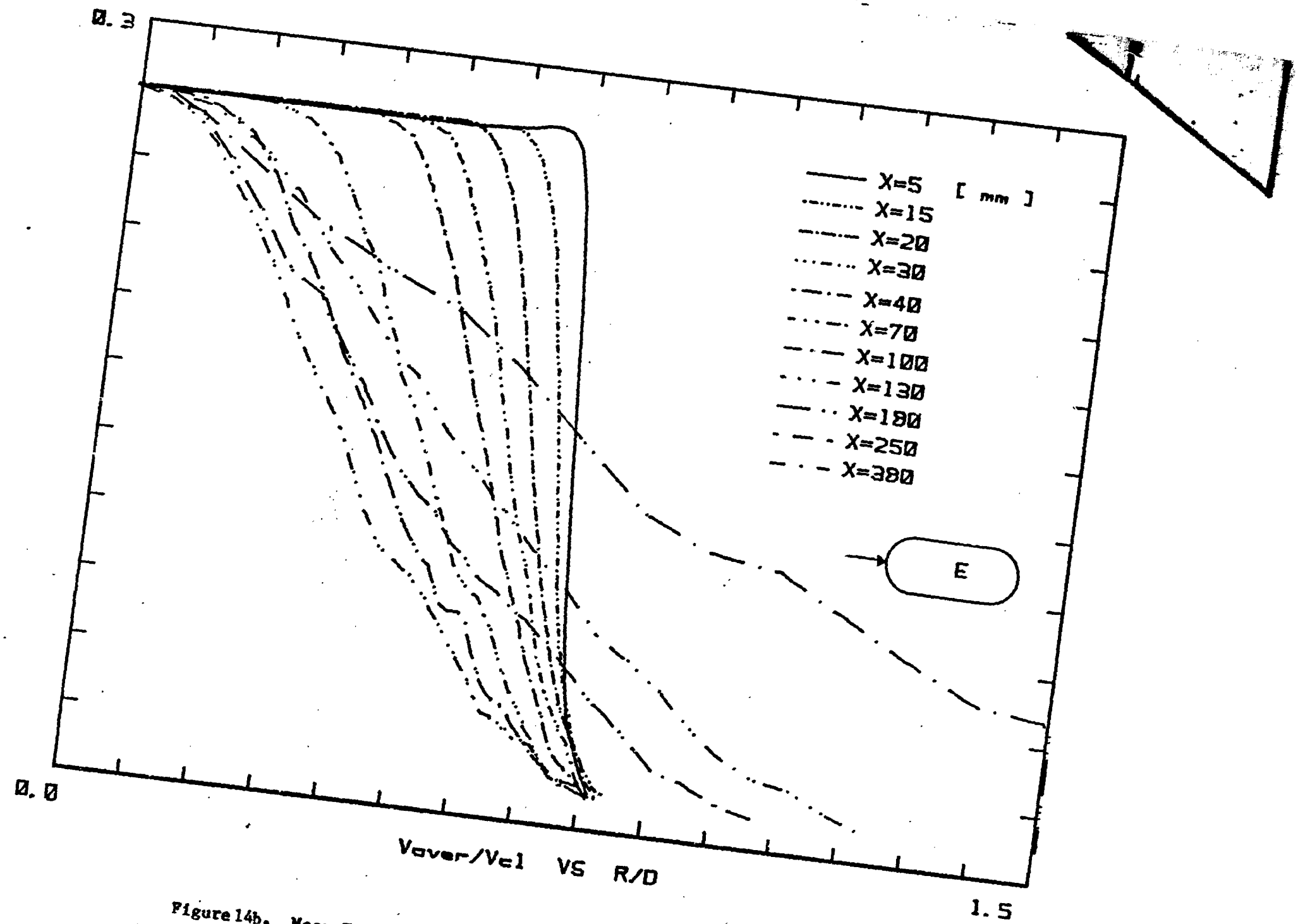

Figure 14b. Mean Velocity Profiles of the Slot-Jet, Major Axis Plane.

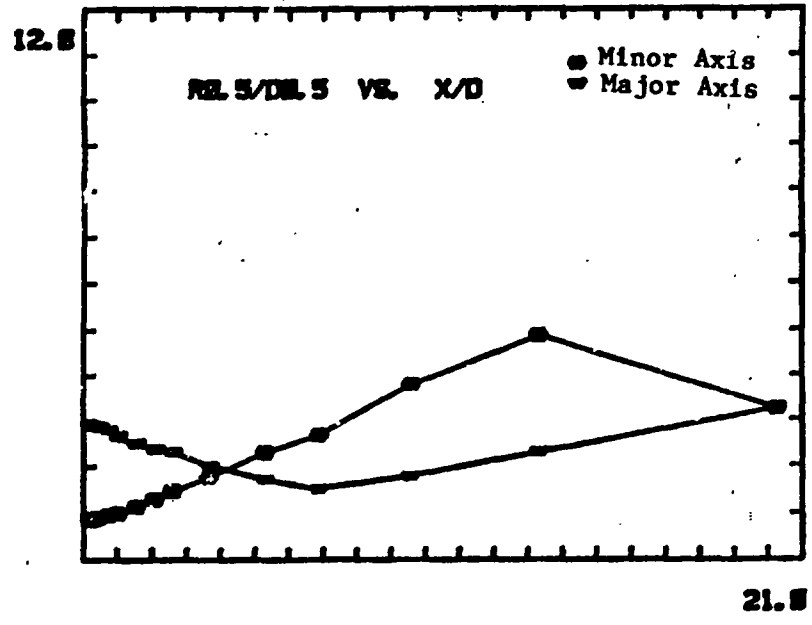

Figure 15. Half Width Variation With Downstream Distance in Slot-Jet.

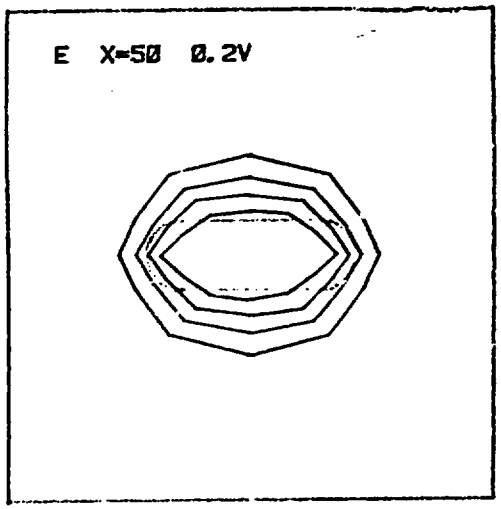
E X=50 0.2V

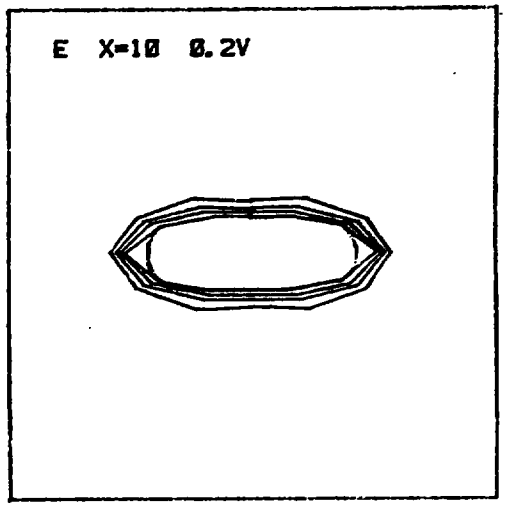
E X=10 0.2V

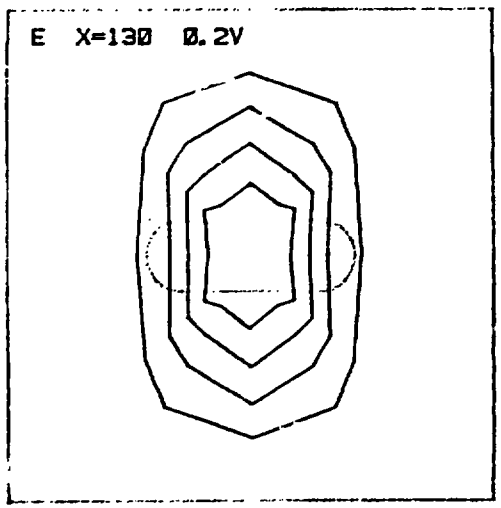
E X=130 0.2V

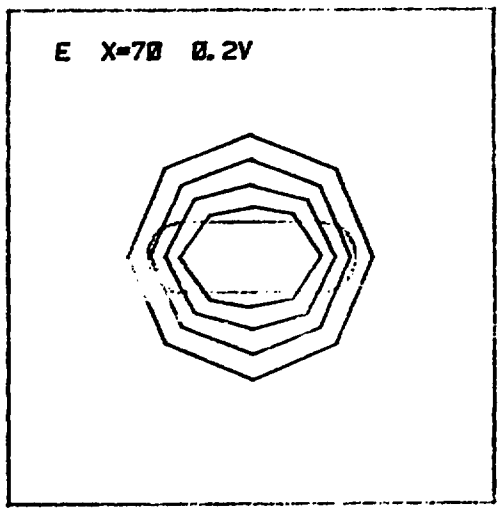
E X=70 0.2V

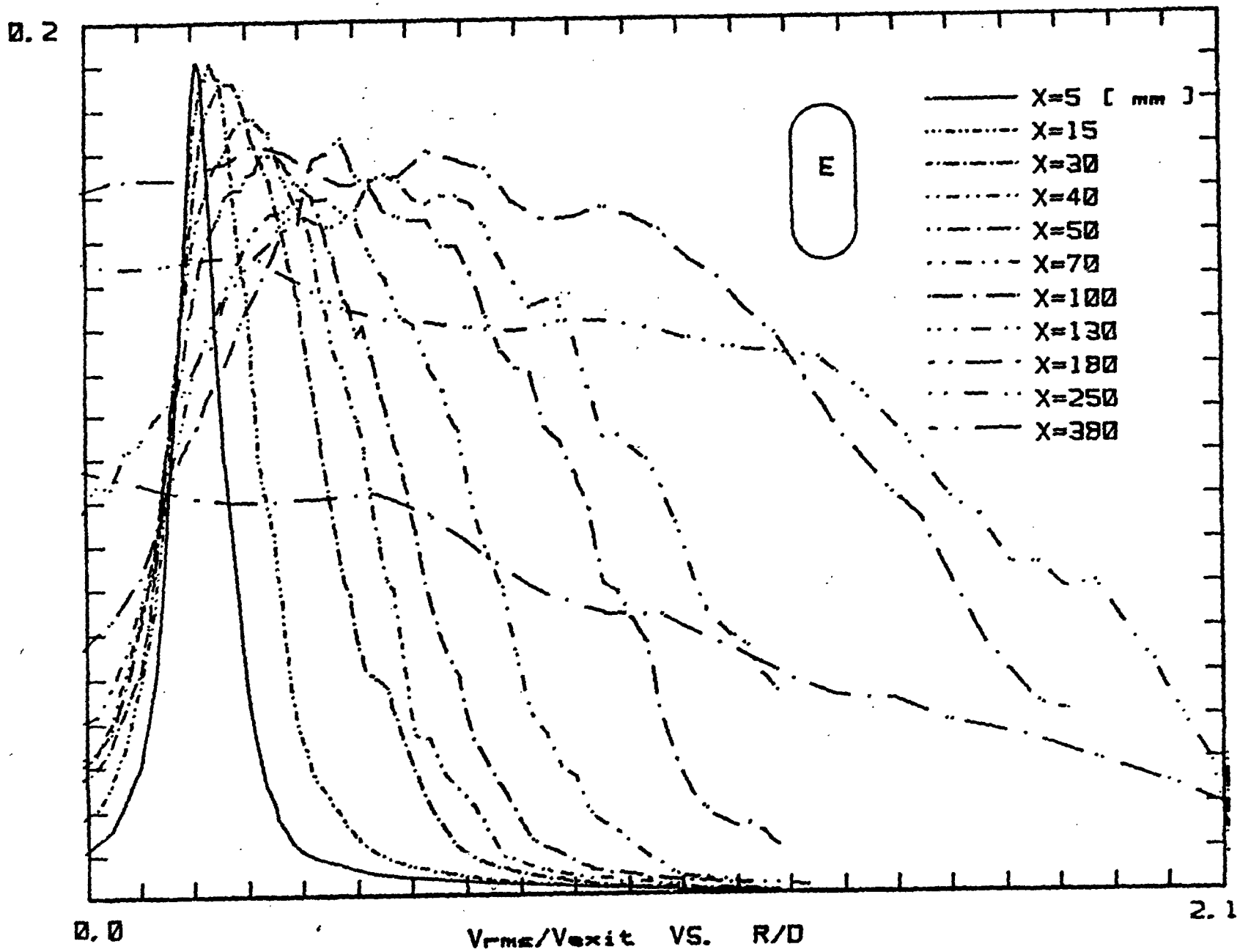

Figure 17a. Turbulence Intensity Profiles in the Slot-Jet, Minor Axis Plane.

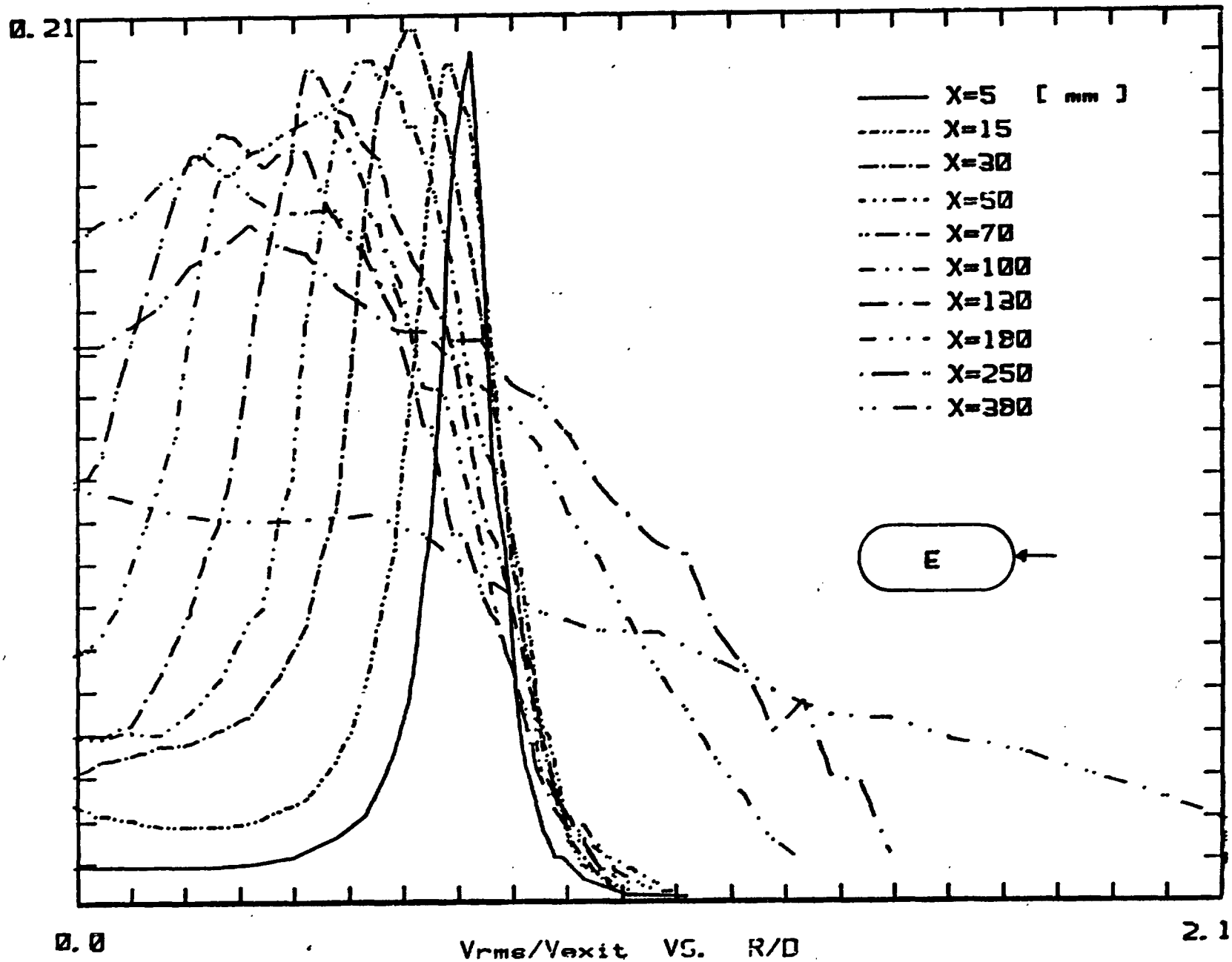

Figure 17b. Turbulence Intensity Profiles in the Slot-Jet, Major Axis Plane.

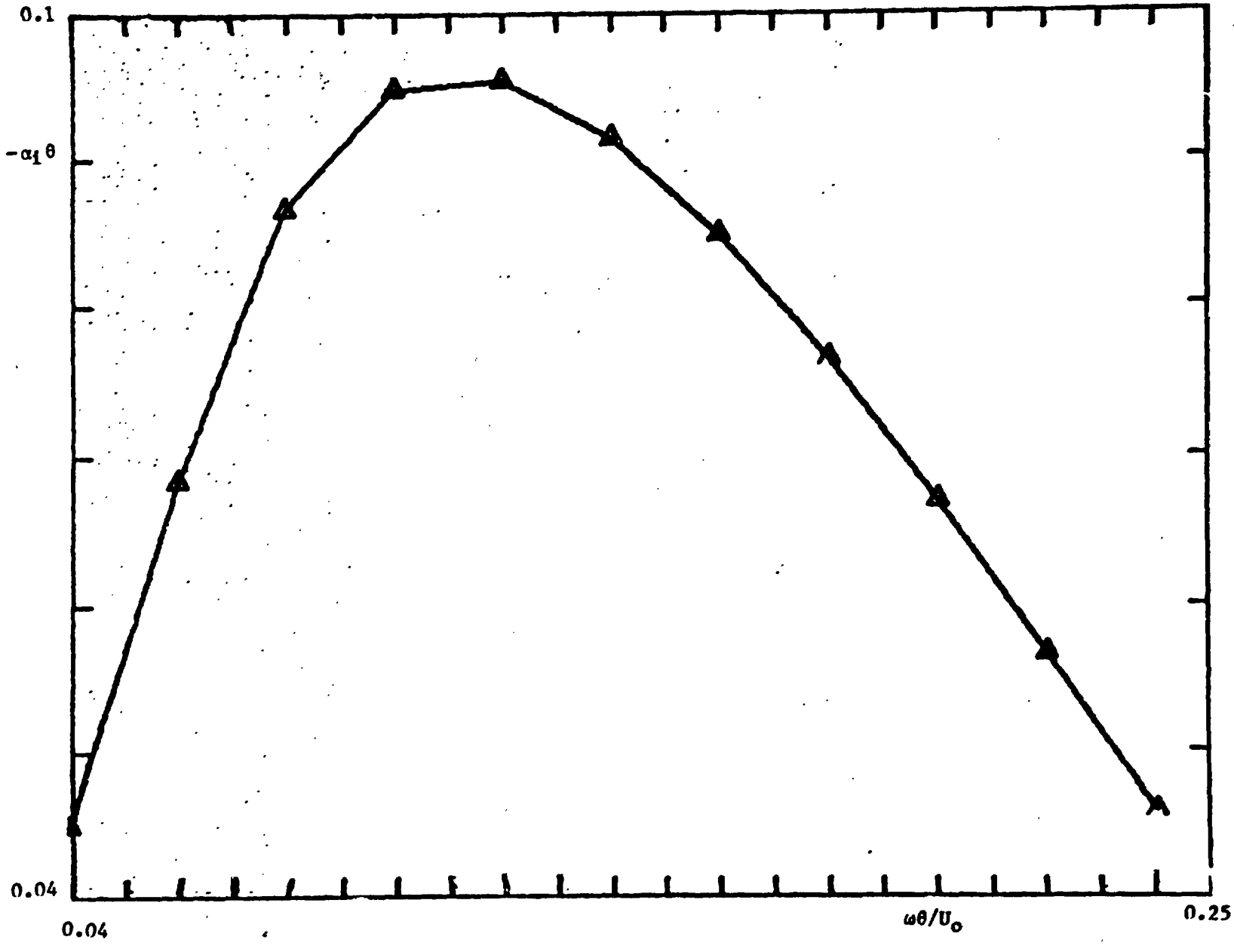

Figure 18. Amplification Curve: Spatial Growth Rate ($-\alpha_1$) dependence on the Strouhal Number $\omega\theta/U_o$.

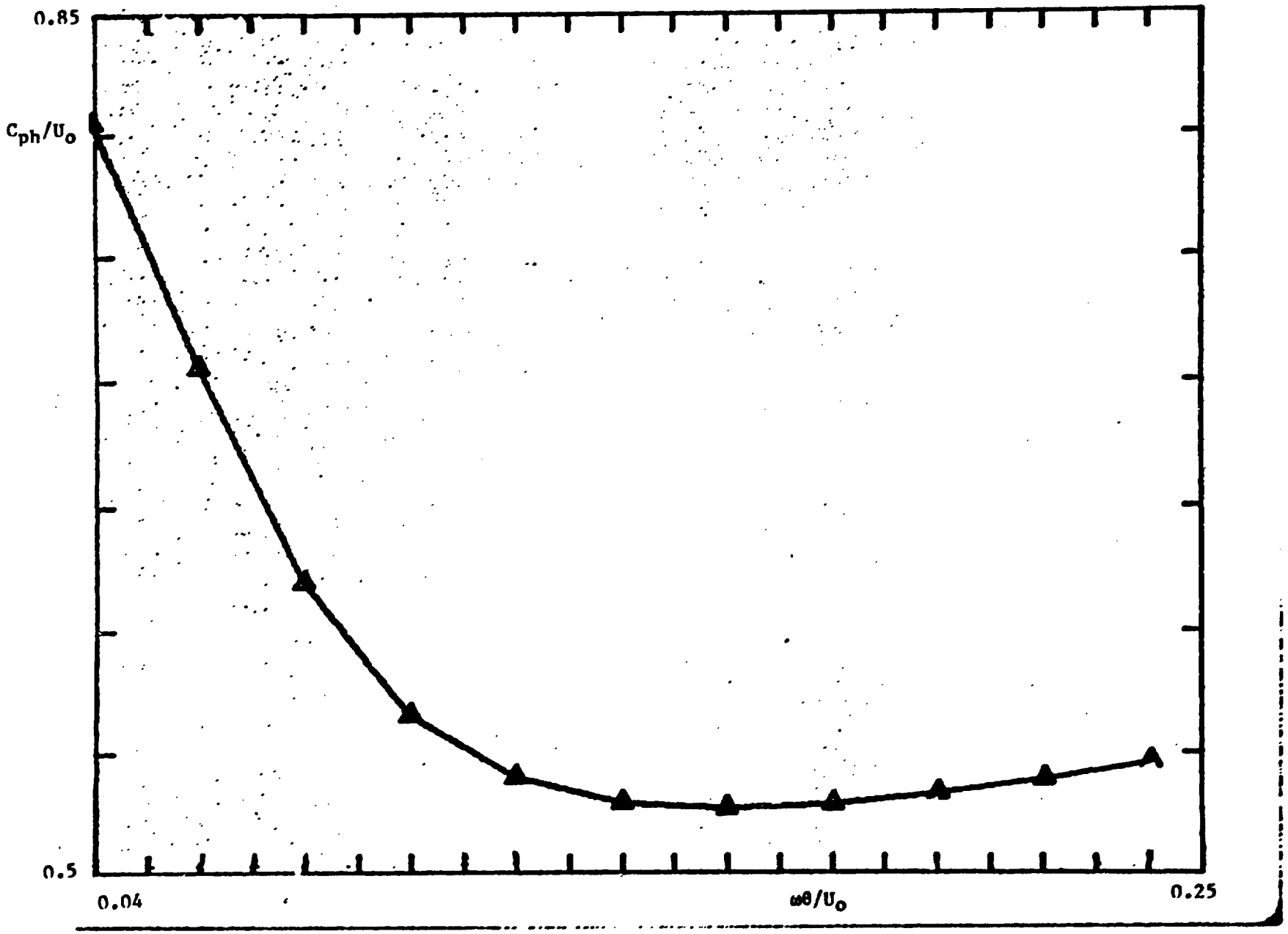

Figure 19. Phase Velocity Variation with Strouhal Number - $\omega\theta/U_o$.

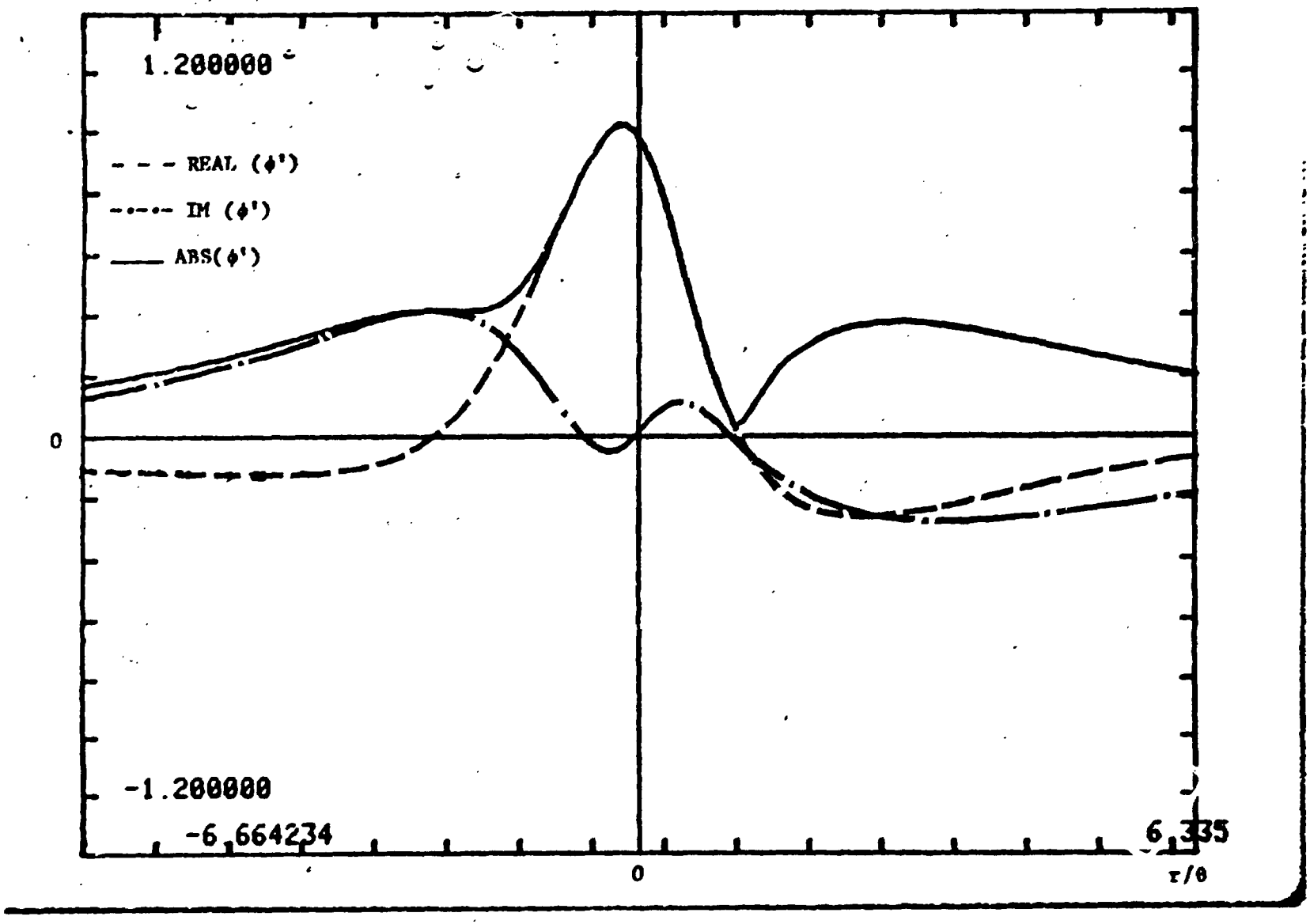

Figure 20. ϕ' Distribution Across the Shear Layer at the Minor Axis Plane.

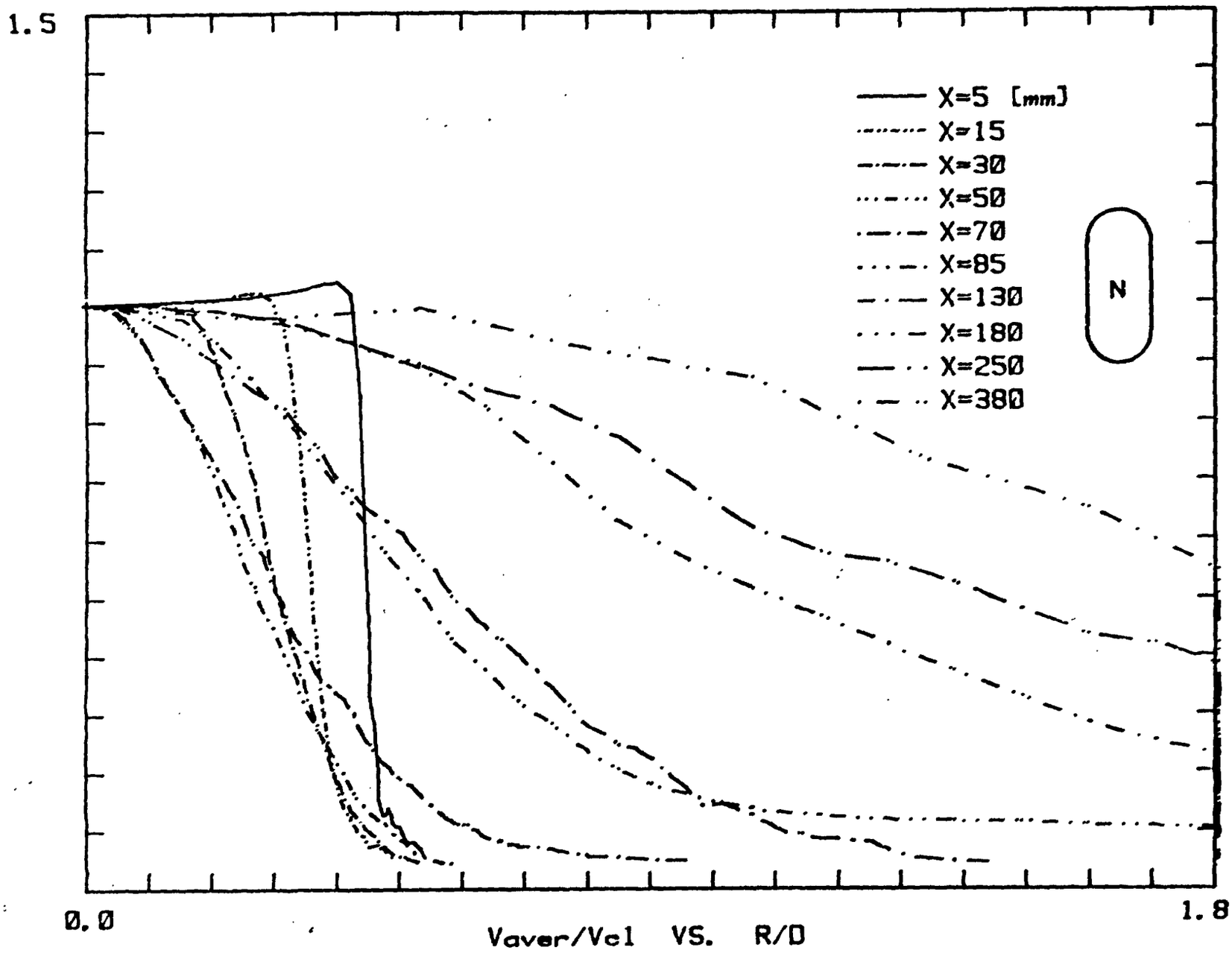

Figure 21a. Mean Velocity Profiles of the Tapered Slot Jet, Minor Axis Plane.

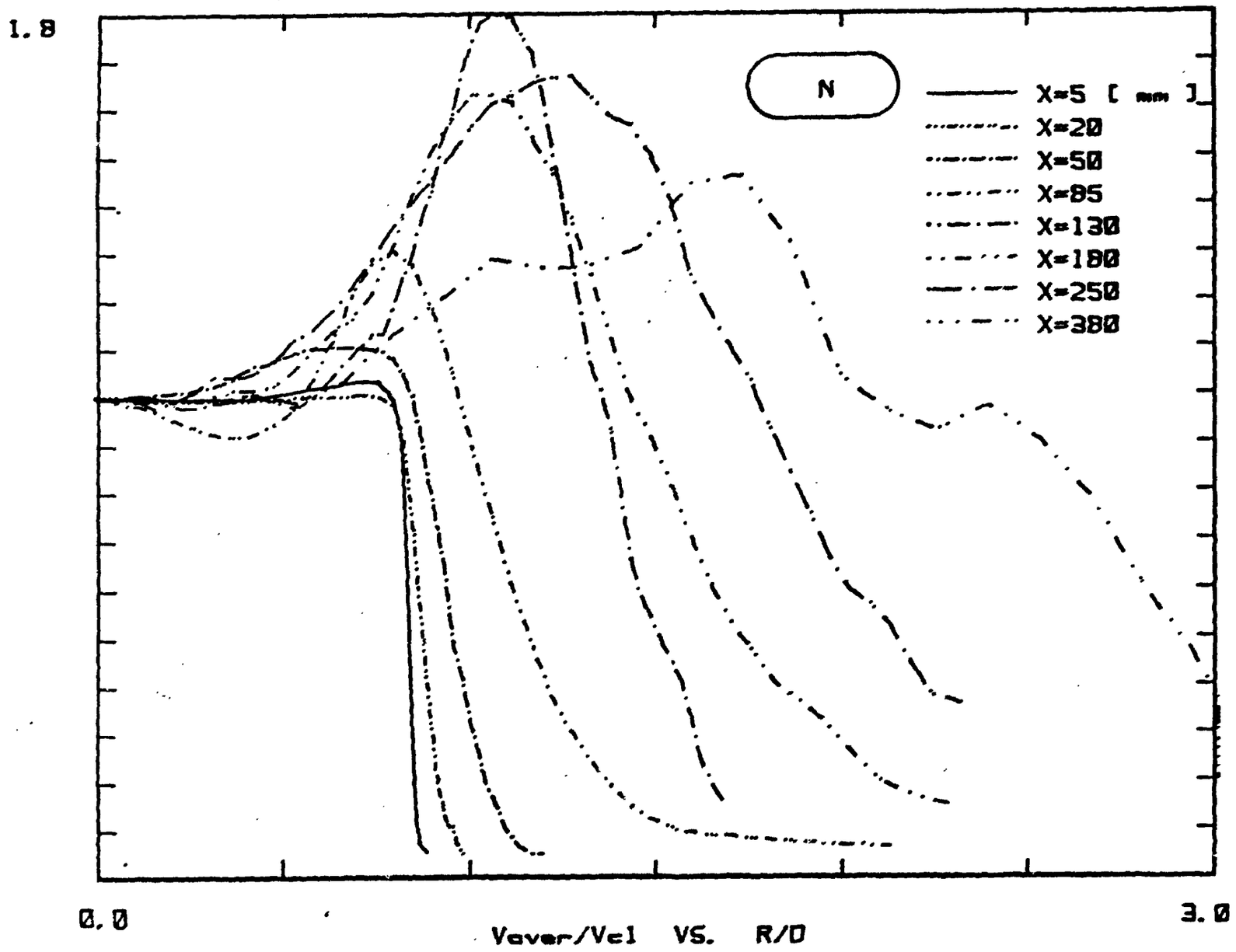

Figure 21b. Mean Velocity Profiles of the Tapered Slot Jet. Major Axis Plane.

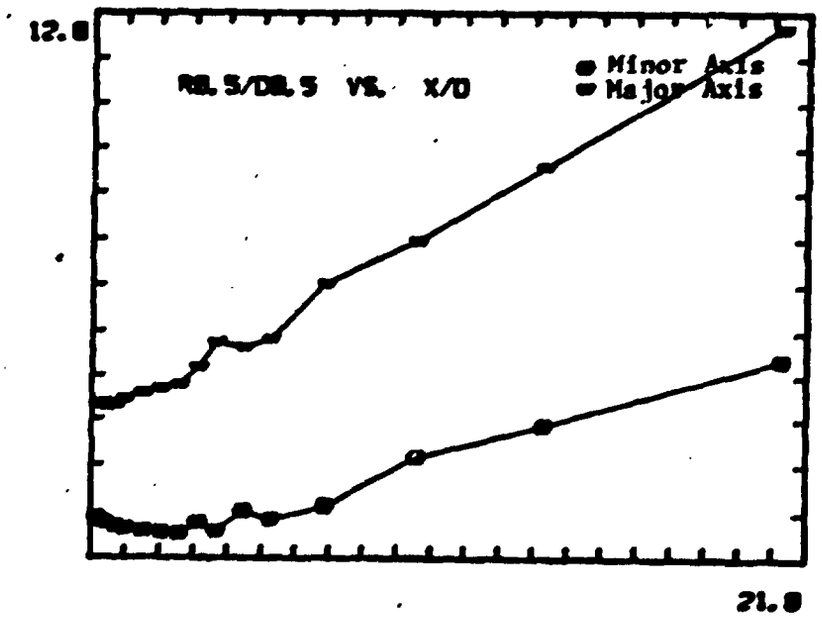

Figure 22. Tapered Slot Jet Half Width Variation with the Downstream Direction.

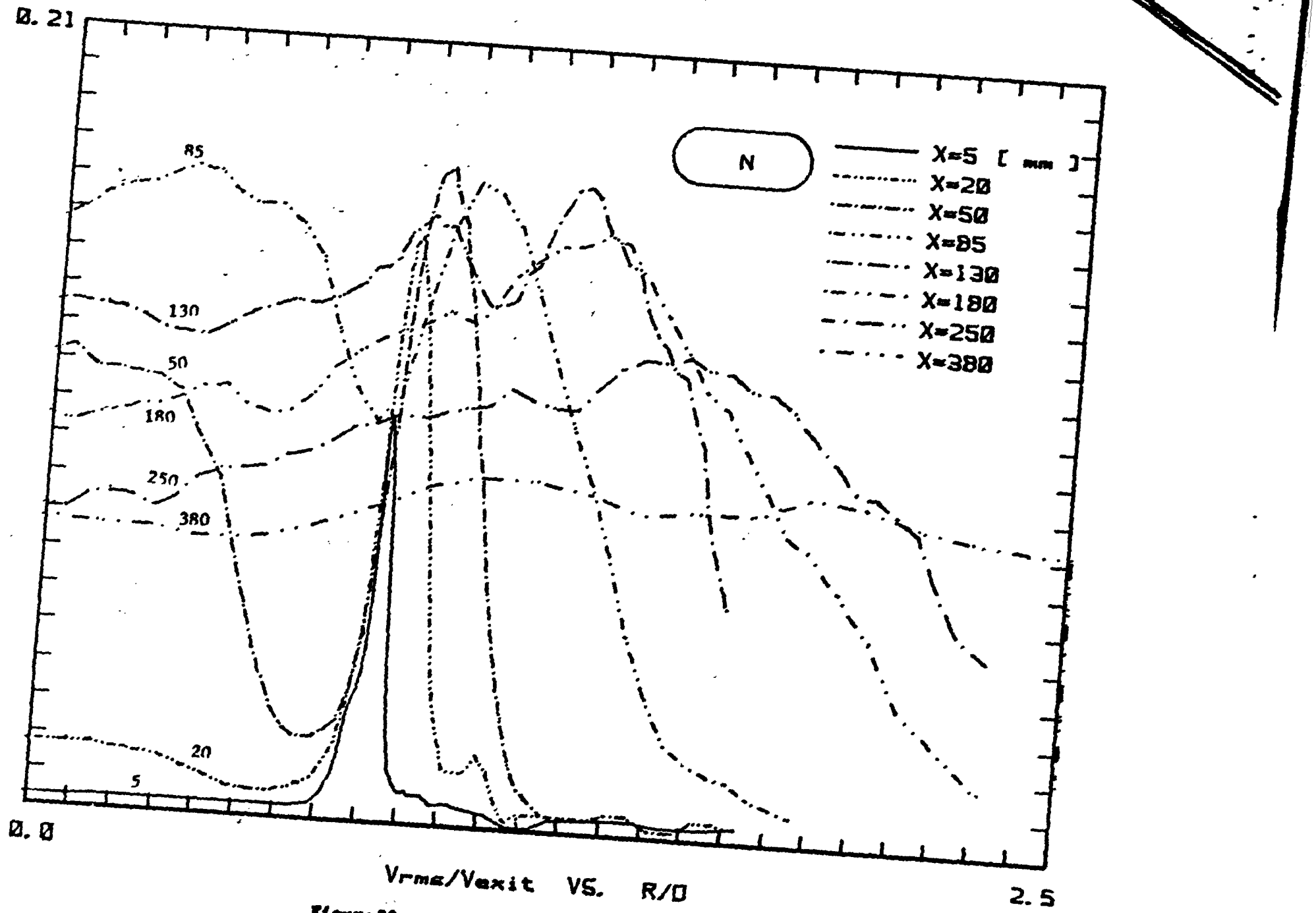

Figure 23a. Turbulence Intensity Profiles of the Tapered-Slot Jet, Major Axis Plane.

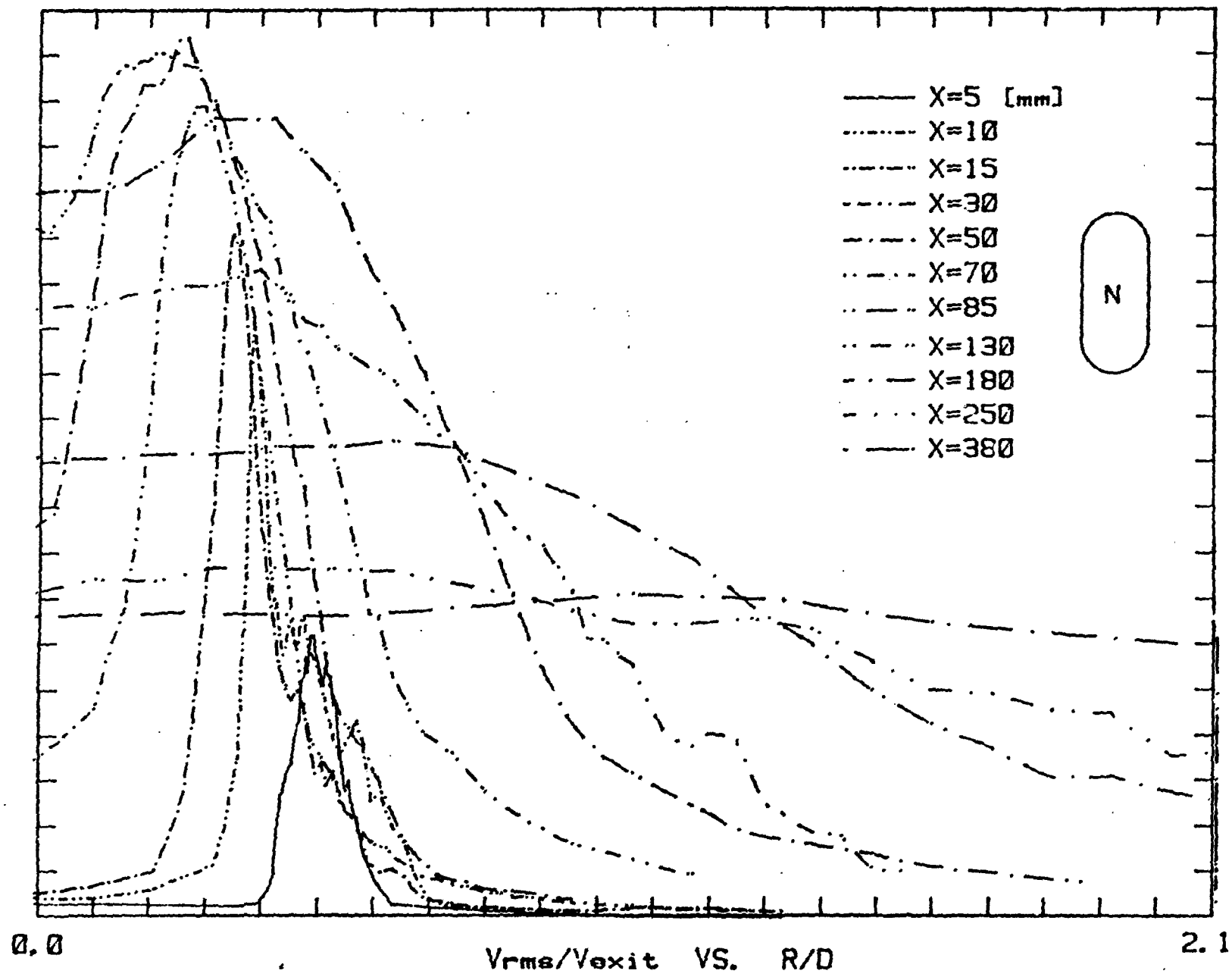

Figure 23b. Turbulence Intensity Profiles of the Tapered-Slot Jet, Minor Axis Plane.

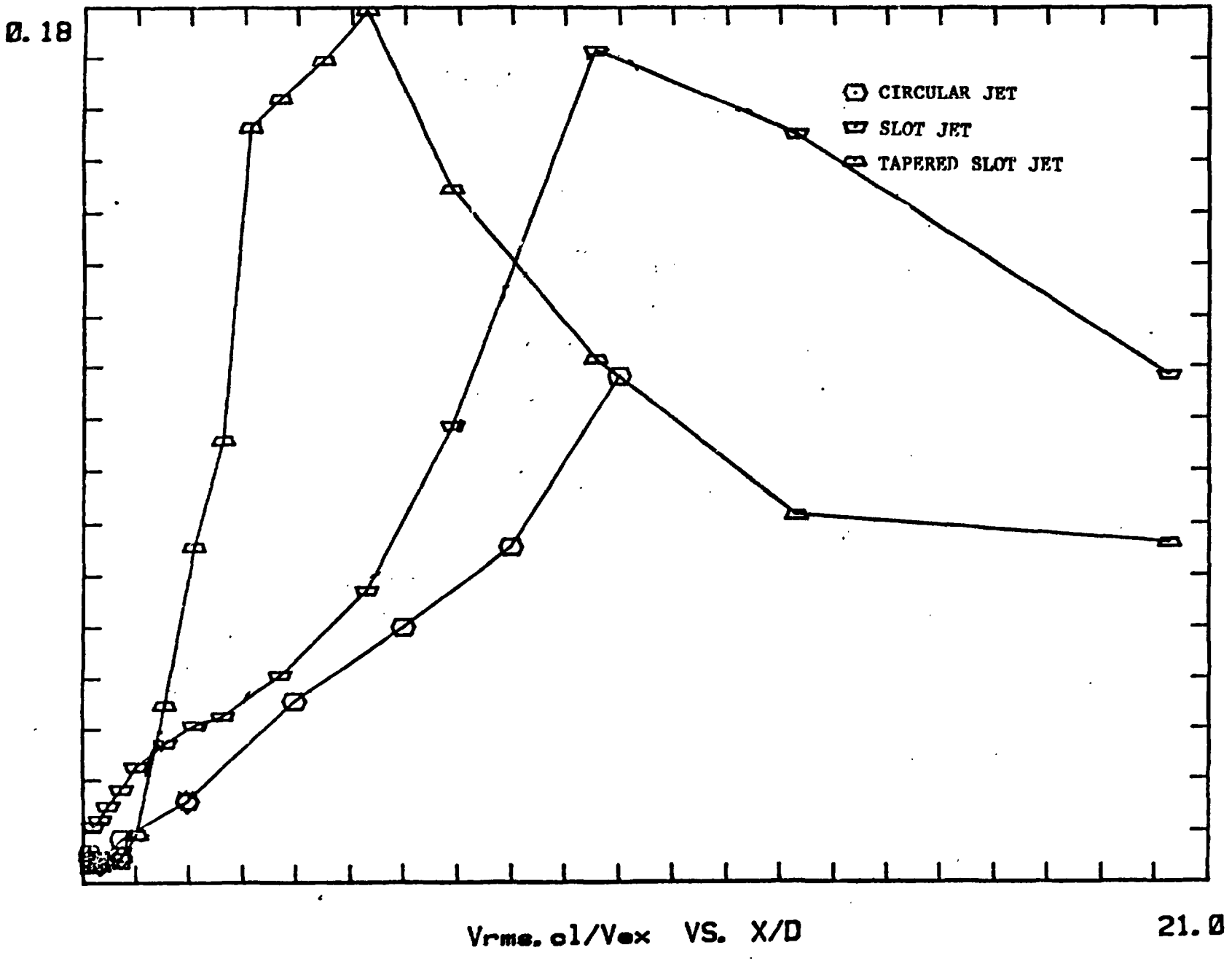

Figure 24. Comparison of the Turbulence Intensity Variation Along the Centerline of the Circular, Slot and Tapered-Slot Jets.

(A) Major axis plane

(B) Minor axis plane

Figure 25: Smoke visualization of the tapered elliptical jet.

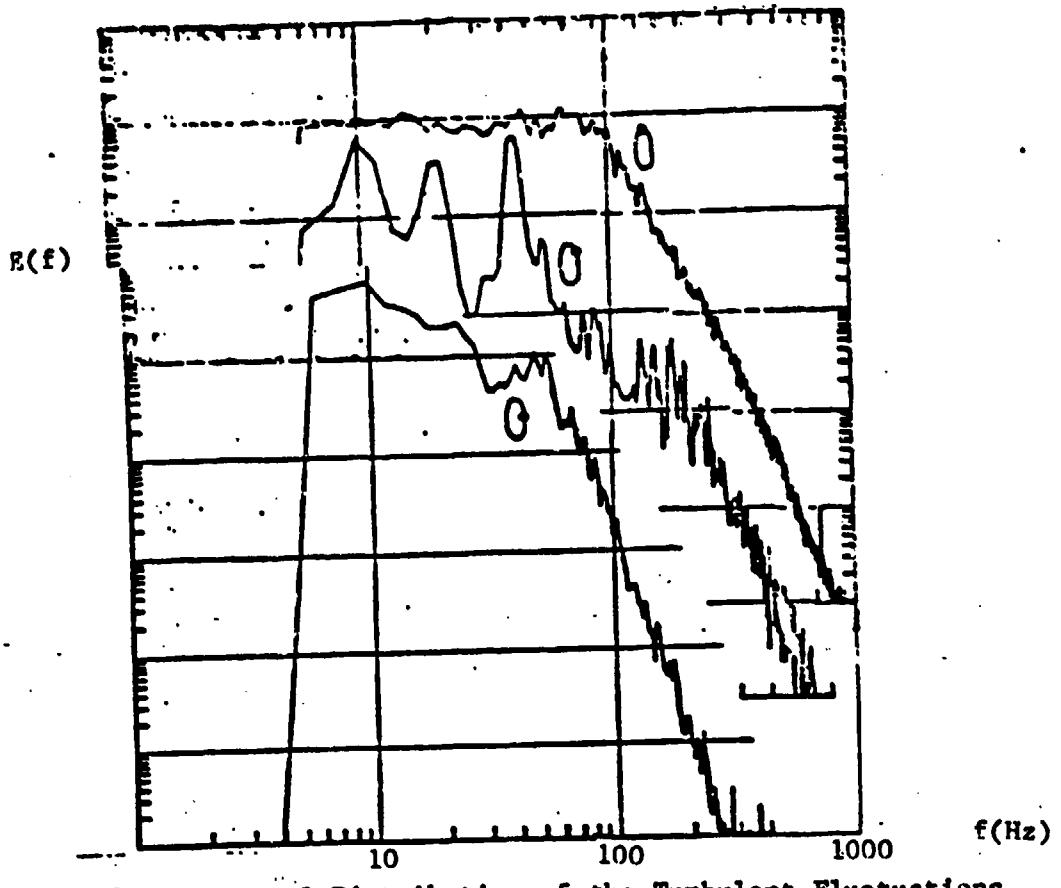

Figure 26. Spectral Distribution of the Turbulent Fluctuations at Three Azimuthal Locations of the Tapered Slot Jet.